KEY ISSUES REVIEW

The physics of jamming for granular materials: a review

IOP Publishing Reports on Progress in Physics
Rep. Prog. Phys. **82** (2019) 012601 (26pp) https://doi.org/10.1088/1361-6633/aadc3c

Key Issues Review

The physics of jamming for granular materials: a review

Robert P Behringer[1,3] **and Bulbul Chakraborty**[2]

[1] Department of Physics & Center for Non-linear and Complex Systems, Duke University, Durham, NC, United States of America
[2] Martin Fisher School of Physics, Brandeis University, Waltham, MA, United States of America
[3] Dr Robert Behringer passed away in July 2018.

E-mail: bulbul@brandeis.edu

Received 13 August 2015, revised 24 July 2018
Accepted for publication 22 August 2018
Published 7 November 2018

Corresponding Editor Professor Sean Washburn

Abstract

Granular materials consist of macroscopic grains, interacting via contact forces, and unaffected by thermal fluctuations. They are one of a class systems that undergo jamming, i.e. a transition between fluid-like and disordered solid-like states. Roughly twenty years ago, proposals by Cates *et al* for the shear response of colloidal systems and by Liu and Nagel, for a universal jamming diagram in a parameter space of packing fraction, ϕ, shear stress, τ, and temperature, T raised key questions. Contemporaneously, experiments by Howell *et al* and numerical simulations by Radjai *et al* and by Luding *et al* helped provide a starting point to explore key insights into jamming for dry, cohesionless, granular materials. A recent experimental observation by Bi *et al* is that frictional granular materials have a a re-entrant region in their jamming diagram. In a range of ϕ, applying shear strain, γ, from an initially force/stress free state leads to fragile (in the sense of Cates *et al*), then anisotropic shear jammed states. Shear jamming at fixed ϕ is presumably conjugate to Reynolds dilatancy, involving dilation under shear against deformable boundaries. Numerical studies by Radjai and Roux showed that Reynolds dilatancy does not occur for frictionless systems. Recent numerical studies by several groups show that shear jamming occurs for finite, but not infinite, systems of frictionless grains. Shear jamming does not lead to known ordering in position space, but Sarkar *et al* showed that ordering occurs in a space of force tiles. Experimental studies seeking to understand random loose and random close packings (rlp and rcp) and dating back to Bernal have probed granular packings and their response to shear and intruder motion. These studies suggest that rlp's are anisotropic and shear-jammed-like, whereas rcp's are likely isotropically jammed states. Jammed states are inherently static, but the jamming diagram may provide a context for understanding rheology, i.e. dynamic shear in a variety of systems that include granular materials and suspensions.

Keywords: jamming, granular materials, friction, soft matter, shear jamming

(Some figures may appear in colour only in the online journal)

1. Introduction

1.1. General overview of granular materials

Granular materials belong to a class of systems that exhibit jamming, i.e. a transition from a fluid-like to a disordered solid-like state that occurs out of thermal equilibrium [1], in the absence of Brownian motion, and that is driven by external forcing such as compression or shear. This review is focused on jamming in systems without any thermal fluctuations, which occurs for collections of macroscopic particles of size larger than a micron. Other members of this class of 'athermal' materials include foams [2], emulsions [3], and non-thermal colloids. Unlike equilibrium fluid–solid transitions, jamming transitions have not been unified under a comprehensive theoretical framework, although a unified jamming phase diagram has been proposed [4] and extensively investigated in the context of frictionless granular particles [5]. Unanswered fundamental questions include: what are the relevant state variables; what role is played by the protocol, i.e. the history associated with the creation of a state; and indeed, what constitutes a well defined state. One source of difficulty in formulating a unified jamming theory is understanding the differences between the collective behavior of systems of particles with or without frictional contact forces between grains, or when particles do or do not have attractive forces such as cohesion. For dry granular materials, the absence of cohesion implies that a granular solid only exists in the presence of externally imposed stresses arising, for instance, from body forces, such as gravity, or through boundary stresses such as compression or shear. The question of rigidity of jammed solids is even more challenging since, unlike thermal matter, the usual notions of excitations and relations between fluctuations and response cannot be easily generalized to jammed solids, most particularly when the particle are frictional. It is the presence of mechanical constraints alone that determines whether a system can resist perturbing stresses, and be mechanically stable, or whether it will deform or flow until mechanical equilibrium is restored: there is no well-defined thermal equilibrium state about which to deform [6, 7]. The point of this review is to consider the nature of jammed granular states, and to understand: how these states arise as functions of preparation history (protocol), friction coefficients; how they behave in response to perturbations, and changes in the collective behavior of jammed states as key system properties are changed. In particular, particle friction and shape play key roles.

1.1.1. Metastability. Granular materials are almost always far-from-equilibrium systems in the thermodynamic sense. When these materials are in a jammed state, they are typically in a local energy minimum, but by no means in the lowest possible energy. A heap of sand on a flat surface is an obvious example: in the absence of external perturbations, it can be stable, but a lower energy state is available where the heap has been reduced to a single layer of grains. Note that if the grains are dry and cohesionless, there are no attractive forces, and hence no surface tension. The heap is stable because the energy available from thermal fluctuations is much too small to dislodge a grain. For instance, at room temperature, the energy needed to lift a 1 mm sand grain off the surface of a heap is $\sim 5 \times 10^{12}$ times greater than thermal energies, $k_{\mathrm{B}}T$. In fact, vibration is often used as a strategy to provide a mechanical analogue to thermal motion in granular materials.

The metastability of granular jammed states is a property they share with other glassy systems, which have fallen out of thermal equilibrium. Like glasses, jammed solids are also amorphous in nature, with no identifiable long-range spatial order. The two classes however differ in that thermal fluctuations are important for stabilizing glasses, whereas they play no role in jamming. In addition, glasses are not defined by contact networks but by positional correlations, whereas the properties of jammed granular states for frictional particles are defined by contacts and contact forces. An infinitesimal displacement of a particle can break a contact and affect a jammed state [8].

1.1.2. Fluctuations. One might be tempted to assume that since temperature has no significant role in granular materials that there would be no fluctuations. In fact, the reverse conclusion applies. Since temperature cannot relax inhomogeneities, granular materials can exist in states with large local variations. When flowing, granular materials typically exhibit large spatial and temporal fluctuations with magnitudes vastly exceeding those of thermal fluctuations [9, 10].

The spatial and temporal scales of fluctuations during flow are at best partially understood, but are certainly sensitive to the nature of the underlying structure of the system. For instance, for slow to moderate shear-rate flows, where forces are carried on force chains, i.e. networks of grains carrying large forces, force fluctuations occur over many tens of grains, at least. In such flows, fluctuations occur with a fastest time of at least $\dot{\gamma}^{-1}$, where $\dot{\gamma}$ is the shear rate.

1.1.3. Coarse graining. Although coarse grained measures such as density or stress show decreasing fluctuations when they are computed over increasing sizes, there is a delicate balance between computing coarse grained continuum measures, and averaging out meaningful spatial gradients [11, 12]. Continuum models posit the existence of a reasonable coarse graining length scale, but there are few [12, 13] direct experimental tests to establish a rigorous coarse graining procedure. The formation of shear bands in granular materials is an example where this matters. Such bands occur routinely as an instability in physical materials that are subject to shear, are no more than a few 10's of grains wide, and are usually significantly less dense than the neighboring material [14]. Once shear bands form, additional strain tends to be localized in the shear bands because their lower ϕ makes them weaker. The propensity to shear band formation presents a particular challenge for drawing conclusions about experimental data, since the response of a system containing shear bands is dominated by the shear band, not the remaining material. It is no longer reasonable to think of the system as having a 'state'. By contrast, numerically simulated systems of frictionless particles may exhibit shear bands, but to our knowledge, these are typically transient, forming in a given location, but then

vanishing and reappearing elsewhere in the system [15]. For our purposes, granular *states* will typically have local fluctuations in density or perhaps other properties. A system that has persistent shear bands or other long range spatial variability cannot be represented as existing in a single well defined state.

1.1.4. Stress tensor. The appearance of contact forces in the description of microscopic configurations indicates the importance of the *local* stress or force moment tensor of each grain [16, 17] in determining the mechanical properties of granular jammed states. Here, we provide a discussion of the relation between the microscopic dynamics of particles and the resulting larger scale fields that arise in continuum descriptions of particulate matter through conservation laws for basic mechanical properties such as mass, momentum and energy. The stress tensor occurs in the context of momentum conservation, and its form is particularly important for statics and dynamics near jamming. As discussed in Goldenberg and Goldhirsch [18], the microscopic momentum density is given by

$$\mathbf{p}^{\mathrm{mic}}(\mathbf{r},t) = \Sigma_i m_i \mathbf{v}_i \delta(\mathbf{r}-\mathbf{r_i}) \tag{1}$$

where the m_i and $\mathbf{r}_i$ are the masses and positions of individual grains, and $\mathbf{r}$ is the position coordinate for the corresponding smoothed field. It is possible to obtain a continuum representation of the momentum density by coarse graining, i.e. convolving, $\mathbf{p}^{\mathrm{mic}}(\mathbf{r},t)$ with an appropriate function, $\phi(\mathbf{R})$ that is unit-normalized, peaked uniquely at $\mathbf{R}=0$ and that has a finite width, w, that sets the coarse graining scale. Assuming that the particles satisfy Newtonian mechanics, the space-time varying continuum momentum density satisfies

$$\dot{p}_\alpha = -\partial[\rho V_\alpha V_\beta - \sigma_{\alpha\beta}]/\partial r_\beta \tag{2}$$

where the dot implies partial differentiation with respect to time, and $\mathbf{V}$, the coarse-grained velocity, is the ratio of the coarse grained momentum density and the coarse grained mass density. The coarse grained mass density is obtained from the microscopic mass density, $\Sigma_i m_i \delta(\mathbf{r}-\mathbf{r_i})$ by coarse graining/convolution with $\phi(\mathbf{R})$. The stress tensor, $\sigma_{\alpha\beta}$, contains two parts:

$$\begin{aligned}\sigma_{\alpha\beta} &= (-1/2)\Sigma_{i,j} f_{ij\alpha}(t) r_{ij\beta}(t) \int_0^1 \mathrm{d}s\,\phi(\mathbf{r}-\mathbf{r_i}+s\mathbf{r_{ij}}) \\ &\quad -\Sigma_i m_i v'_{i\alpha}(\mathbf{r},t) v'_{i\beta}(\mathbf{r},t)\phi(\mathbf{r}-\mathbf{r}_i),\end{aligned} \tag{3}$$

where the fluctuating velocities are $v'_\alpha(t) = v_\alpha(t) - V_\alpha(\mathbf{r},t)$ and $V_\alpha(\mathbf{r},t)$ is the local coarse grained velocity. The first term on the right side of equation (3) is the contact or collisional stress, and the second term is the kinetic or streaming stress. The former is important for static or slowly evolving systems. The latter dominates for stiff particles and in rapid flows where contacts are short-lived. Similar relations can be derived for energy conservation, and for the familiar continuity equation that expresses mass conservation.

The partitioning of the stress tensor into *contact* and *kinetic* parts, and the effect of dimension, d and friction coefficient, μ, on the mean number of contacts per particle, z needed for mechanical stability (discussed below) provide means of effectively partitioning granular systems into broad classes. There is a continuum of friction coefficients and particle stiffnesses, hence of z_{iso}'s and of relative importance of the two stress components. Nevertheless, we expect that near jamming, vastly different behavior is associated with frictional versus frictionless spheres, with rapid versus slow flows or static states, and infinitely hard particles (inherently collisional) versus deformable particles.

A particularly relevant example of a phenomenon that pertains to a given class is force chains. For frictional deformable particles and slowly sheared quasi-static systems, force chains are long-lived [19–22]. Although force-chain-like networks can occur for hard or slippery particles, they are dynamic phenomena because force chains are generically unstable for frictionless spheres or disks. A particularly interesting question concerns crossover in behavior between low, moderate and high friction, and between situations where different parts of the stress tensor dominate. In this review, we are primarily concerned with the effects of friction in the regime where the contact stress dominates.

1.1.5. Statistical mechanics of jamming. Given that granular materials are characterized by large fluctuations, it is clear that they should be analyzed statistically, and that jamming should be studied as the emergence of collective behavior from a large number of interacting microscopic entities. This forces us to address difficult questions about statistical ensembles, history dependence, or protocol, and the effects of disorder. Because of frictional contacts, forces are not derivable from a potential energy that depends only on the particle coordinates, and hence the microscopic configurations of static granular assemblies cannot be completely characterized by just the positions of the grains. The forces depend on the 'history' of preparation. However, one could enlarge the notion of a microstate to include the contact forces to eliminate this history dependence at the expense of creating a new kind of statistical ensemble and be faced with the task of constructing a statistical mechanics based on such an ensemble. This approach was pioneered by Edwards and a number of collaborators [17, 23–25] and has been developed over the last couple of decades [26]. A review appears in [27]. The notions of order parameters, correlation lengths and response functions, associated with phases and phase transitions in equilibrium fluid–solid transitions therefore, need to be reexamined in the context of such an ensemble.

1.2. Contact and force networks

As noted, dry granular systems are cohesionless, and grains interact via purely repulsive contact forces. Since thermal fluctuations are absent, there is no smoothing out of the effects of contact breaking (and forming). The distinction between fluid-like states and jammed states is, therefore, all about the properties of the contact network and the contact forces that collectively satisfy the constraints of static mechanical equilibrium. In a jammed state, force and torque balance have to

be strictly satisfied at the level of every grain (with the exclusion of rattlers), and this imposes strict requirements on the contact network [28–31]. Unjamming occurs when the density or shear stress reaches a limit beyond which these local constraints can no longer be satisfied. With purely repulsive contact forces, it is not possible to create an isolated region of grains in contact via non-zero forces: any such region has to percolate to the boundaries. Unjamming or jamming thus has to be a collective phenomenon, where changes in macroscopic observables associated with the contact network and force network necessarily accompany these transitions.

1.2.1. Rattlers. A jammed granular material has some subset of particles, non-rattlers, that are in mechanical equilibrium, i.e. in force and torque balance. A coexisting subset of particles, rattlers, consists of all particles that are not mechanically stable. Except just at jamming, systems of particles that are jammed, have mechanical rigidity in that they can resist non-zero applied stresses, although the applied forces that can disrupt a jammed state can be very small if the system is close to jamming.

1.2.2. Isostaticity. One way to think about the restrictions placed on contact networks by the constraints of packing and of mechanical equilibrium is by counting the degrees of freedom, commonly referred to as the Maxwell counting arguments [28, 29, 32]. The constraints of force balance in d dimensions leads to d equations per grain. The condition of torque balance provides an additional $d(d-1)/2$ equations per grain. The unknowns are the contact forces. If the total number of contacts in a packing of N grains is $Z_{\rm tot} \equiv zN$, we have $zN/2$ unknown vector forces since each contact force is shared by two grains.

For frictionless systems with purely normal forces, the torque balance equations are trivially satisfied and we have $zN/2$ variables constrained by dN equations. For a solution to exist, $z \geqslant 2d$. Isostatic packings are ones that satisfy the equality condition with $z_{\rm iso} = 2d$, and packings with higher z are hyperstatic. For nonspherical grains, the isostaticity argument has to be revisited and it can be shown that hypostatic packings with $z < z_{\rm iso}$ are stable [33–36].

The isostaticity argument can be extended to frictional grains with friction coefficient μ, by including the torque balance conditions *and* by adding an additional attribute to a packing, which is the fraction of contacts, q that are fully mobilized with the tangential force f_t saturating the Coulomb bound $|f_t| = \mu f_N$. The Maxwell counting argument can then be generalized. The number of unknowns is $(\frac{zN}{2}(q(d-1)+(1-q)d)$ and the number of constraints is $\frac{Nd(d+1)}{2}$. The isostatic condition, therefore, reads $z_{\rm iso} = \frac{d(d+1)}{(d-q)}$. This extended Maxwell argument agrees well with observations in numerical simulations [37]. It is clear that $z_{\rm iso}$ for frictional grains is not just determined by dimensionality but depends on q and, therefore, how the packing was prepared. In the limit of $\mu \to \infty$, $q = 0$ and $z_{\rm iso} = d+1$, which is also a lower bound on the frictional isostatic contact number. This generalized argument can only be applied at finite μ: the frictionless case cannot be obtained as a limit of $\mu \to 0$. Specifically, setting $z_{\rm iso} = \frac{d(d+1)}{(d-q)}$ to the $\mu = 0$ value $z_{\rm iso} = 2d$ leads, in general, to unreasonable values of q.

Since for grains that are close to the hard particle limit, the original implementation of the packing constraints is through the rigid sphere constraints: the distance between the centers of two particles in contact has to equal the sum of their radii. An upper bound on both the frictionless and frictional values of $z_{\rm iso}$ can be obtained in this limit. The hard particle constraint provides $zN/2$ constraint equations for dN unknowns, the positions of the particles and a solution can be obtained only when $zN/2 \leqslant dN$, or $z \leqslant 2d$. Putting it all together, for frictional grains, $(d+1) \leqslant z_{\rm iso} \leqslant 2d$. For frictionless, hard disks, $z_{\rm iso} = 2d$ since there is only one value at which the two sets of constraints can be satisfied. This is the special frictionless jamming/unjamming point that occurs at $\phi = \phi_{\rm J}$ and has been discussed extensively as an example of a marginally jammed solid [28, 30].

The Maxwell counting argument, from which the above values of values of $z_{\rm iso}$ are derived, is valid in the absence of special correlations in particle positions. For instance, hard, frictionless disks can crystallize into a hexagonal packing. With or without friction, perfectly straight lines of particles can be in force and torque balance, and therefore regular two dimensional arrays of particles can have z as close as desired to $z = 2$. However, such structures are unstable to small random force perturbations, typically involve some specific correlation, and have minimal probability of occurring in nature. For systems of frictional discs, $z_{\rm iso}$ is empirically found [38–40] to be a bit larger than $d+1$, and in simulations, there is also an accumulation of contacts where the frictional forces lie at the limit of the Coulomb condition [37]

1.2.3. Force networks. Contact networks consist of those particles that share contacts. Force networks are built on top of the contact network, and consist of particles that also experience force at or above a chosen amount. A hallmark of jammed granular solids is that stress is transmitted in a highly heterogeneous manner described by the force networks [6, 41]. Conventionally, there are two types of measures used to quantify the heterogeneity: (a) the distribution of the magnitude of the contact forces is broad and exhibits an exponential tail [14, 21, 40, 42–44], and (b) spatial localization of stresses on a subset of grains [6, 14, 21, 41, 45–47]. The latter phenomenon is particularly noticeable in shear-jammed states of frictional grains in which there is a large number of 'spectator' particles [7], which form a bath for the force-bearing grains [38]. The force networks have been difficult to characterize by two-point spatial correlation functions [48, 49]. There has been an intensive effort from several groups to use network and topology tools to characterize granular networks, and their connection to macroscopic system properties [50–60]. Recent work has shown that there is an alternative representation of the forces in a network that is dual to the real-space network [61, 62], and this representation in two-dimensional systems can be used to quantify the extent of spatial localization of forces. Understanding the nature of

jammed states and the jamming transition requires analysis of both the real-space and force-space networks, which are not simply related in frictional systems.

1.2.4. Rigidity. The above discussion is focused solely on the conditions imposed on a network by the constraints of static mechanical equilibrium. The question of *rigidity* of a jammed state has to be carefully considered. A network of contact forces in static mechanical equilibrium has to satisfy the following grain and contact scale constraints: (i) force balance, (ii) torque balance and (iii) the Coulomb condition restricting tangential forces, f_t to $f_t \leqslant \mu f_N$, where f_N is the magnitude of the normal force and μ is the friction coefficient. Such a network may or may not be stable to an external perturbation and the response depends critically on the magnitude of the additional imposed stress and how compatible the perturbing stress or strain is with the existing force network. For instance, a network that has force bearing grains only along the compressive direction cannot support even an infinitesimal strain in the dilational direction [7]. Shear jamming [38] of frictional grains, discussed in section 4, clearly demonstrates the difference between the responses of fragile and shear-jammed states. The shear-jammed states are rigid to shear reversal but the fragile states are not. Theoretically, the question of rigidity of jammed granular solids poses many challenges. In thermal equilibrium, shear-rigidity is the characteristic that distinguishes crystalline and amorphous solids from fluids. The emergence of rigidity in these systems is a consequence of broken translational symmetry [63]. Granular solids in the absence of thermal fluctuations cannot be characterized in the same way because of the large number of metastable states and the absence of a well-defined zero-stress solid [7]. The rigidity, therefore, depends on the stress imposed to create the state. Theoretical analysis of shear-jammed states indeed show a symmetry breaking, but in the force network that is dual to the real space network [61, 64].

As commonly used, jamming is actually two distinct problems: jamming and unjamming. The former describes the transition between fluid states that cannot resist shear to solids that can. If the grains are modeled as hard spheres, jamming is concerned with the kinetic part of the stress tensor and, jamming is the transition at which the system cannot be compressed any further without creating overlaps of grains: the kinetic pressure diverges but the contact stresses are strictly zero. It is important to note that interactions between dry cohesionless grains do not have tensile strength and respond only if there is compression.

The unjamming process occurs under decompression, and is the mirror image of jamming. It refers to the transition from a solid to a fluid, which is marked by the vanishing of shear modulus. This transition has been thoroughly investigated for frictionless, soft spheres [44].

2. Isotropic versus anistropic jamming: early work

Pioneering theoretical work on jamming was carried out by Cates *et al* [7] who hypothesized models of sheared, athermal colloidal systems and by Liu and Nagel [4] who hypothesized a universal jamming diagram. The former authors proposed that force-chain-like structures, sketched in figure 1, consisting of roughly linear sets of particles that carry much of the applied stress, form in sheared colloids, and that these structures are *fragile*, resisting continued shear in the original compressive direction, but falling apart under reversal of shear. These authors also considered the fragility of sandpiles and the role of the friction angle.

We note that shear may be carried out by deforming a systems boundaries in various ways, as sketched in figure 2. No matter which protocol, shear involves compression along one direction, expansion (dilation) in the perpendicular direction, and possibly an affine rotation. Pure shear consists of just dilation/compression; simple shear involves an additional rotation. Couette shear resembles simple shear in a curved geometry, and consists of shearing in a cylindrical or circular geometry where the relative motion of the curved boundaries have an opposite sense. Necessarily, shear is volume (area in 2D) conserving.

Liu and Nagel first hypothesized a universal jamming diagram, sketched in figure 3 for systems that include colloids, foams, granular materials, glass formers, and other systems that form disordered solids. The Liu–Nagel phase diagram incorporated a non-equilibrium axis measuring shear stress (τ) to the traditional phase space spanned by density (or packing fraction ϕ) and temperature (T). The granular (athermal) part of this phase diagram is spanned by packing fraction and shear stress ($\phi - \tau$) whereas thermal systems undergoing the glass transition live on the $T - \phi$ plane. This jamming diagram was proposed by Liu and Nagel as a way to unify the dynamical glass transition with the purely athermal jamming transition into one class of fluid-disordered solid transitions with a special point at ($\phi = \phi_J, T = 0, \tau = 0$).

Contemporaneous experimental studies by Howell *et al* [20, 21, 65, 66] showed the existence of a jamming transition that contained features of both the Cates *et al* shearing response [7] and a density dependence that controlled the transition between jammed and unjammed states. These experiments, discussed in more detail below, used photoelastic discs that were sheared in a Couette geometry. To our knowledge, it was the first use of photoelasticity to provide particle-scale force data. This system was also modeled by Luding *et al* [65] in an early application of discrete element (DEM) simulations to a granular material near jamming. An image from the experiments, figure 4, shows a network of complex strong force chains, in the spirit of Cates *et al* that are aligned preferentially along the compression direction of the shear. This figure uses a color map of photoelastic response, where red indicates strong force, and blue weak or no force. Experiments discussed below, [39, 68] and shown in figure 5, exemplify the fragile and shear jammed states.

Numerical studies have since focused on the special point, ϕ_J corresponding to the lowest packing fraction for which isotropic jammed exists, to understand the jamming transition in *frictionless* grains and its relationship to the glass transition [5, 44, 69–73]. These studies support the proposed jamming diagram of Liu and Nagel to some extent. However numerical studies of rheology clearly indicate that the limits

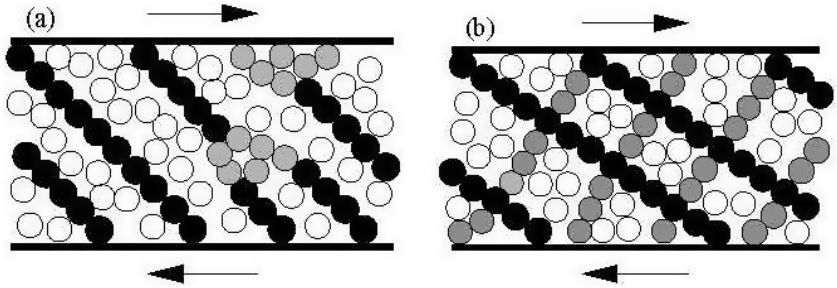

Figure 1. Sketch of force chains of hypothetical force chains in a sheared colloidal system, after Cates *et al* [7] These authors argued that force chains would form along the compressive shear direction (here with slope −1). These force chains would resist continued shear in the original direction, but there would be no strong force network that could resist shear if its direction were reversed (a) force chains along the compressive direction that can resist continued shear only in the original shear direction; (b) continued shearing leads to a two-dimensional force network, which can resist shear reversal.

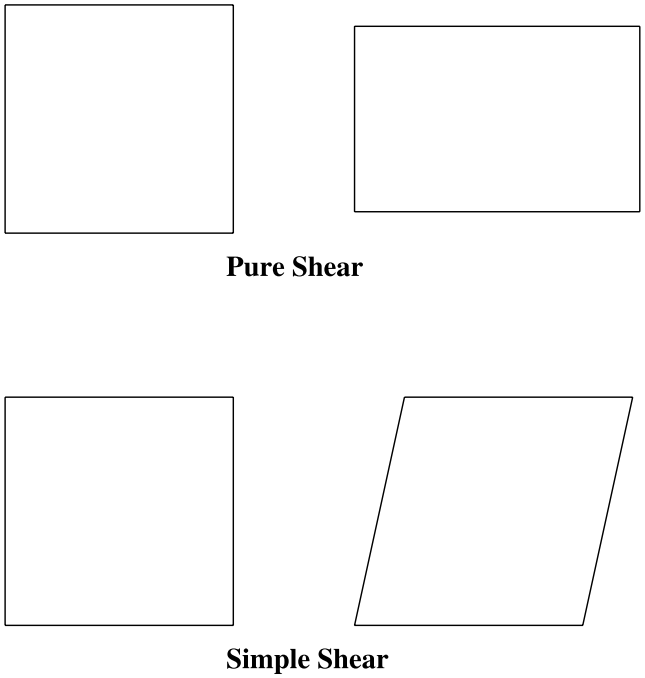

Figure 2. Two common forms of shear strain. Top shows a schematic of pure shear consisting of compression in one direction and equal dilation in the other, keeping the system area fixed. Bottom shows simple shear which corresponds to deforming a rectangle into a parallelogram, at fixed area. An additional common way to apply shear is in a Couette geometry, as in figure 4. In this geometry, the inner out and outer boundaries of a pair of cylinders (rings in 2D) rotate relative to each other.

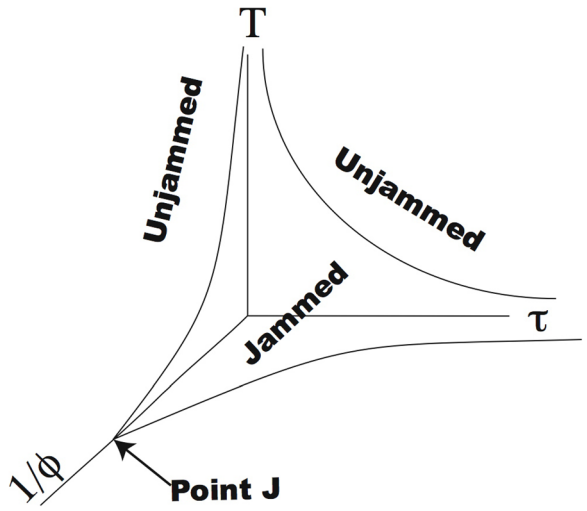

Figure 3. Adaptation of the Liu–Nagel jamming diagram [67]. In the proposal of Liu and Nagel [4], jammed states exist near the origin of a parameter space with axes T, temperature, τ, shear stress, and ϕ^{-1}, inverse packing fraction. This diagram is a proposed unification of glassy systems, for which the thermodynamic temperature is relevant, and granular systems, for which temperature is not. The latter exist in a parameter space consisting of τ and ϕ^{-1} only.

of shear rate going to zero and temperature going to zero are not interchangeable [72, 74]. Granular materials live in the $T = 0$ plane, forcing us to always take the limit in the order of first $T \to 0$ and then the shear rate $\dot{\gamma} \to 0$, whereas the quasistatic shear response of glasses belongs to the class of talking the limit of $\dot{\gamma} \to 0$ before taking $T \to 0$. For isotropically compressed frictionless particles, the work of O'Hern *et al* [44] indicated a unique jamming density density $\phi = \phi_J$ (for a given particle type), and a critical point at zero stress and $\phi = \phi_J$. Subsequent work [75] has shown that the value of ϕ_J can depend on protocol and particle friction coefficient, μ but the properties of this special point are robust. Silbert [76] has computed the jamming packing fractions and values of z_{iso} for isotropically compressed discs and spheres, as shown in figure 6. For small μ, these quantitites differ little from the $\mu = 0$ values. However, for very large friction, $\mu > 1$, both ϕ and z at jamming are measurably smaller. The low and high μ limits are joined by a sigmoidal curve.

2.1. Insights from 2D experiments

Two dimensional (2D) systems, particularly where the particles are photoelastic, provide a powerful approach to understanding the nature of granular systems in general and in particular near the jamming point. The use of photoelastic granular particles was pioneered by Wakabayashi [77] and Dantu [78], and was used to understand soil mechanics by Drescher and Josselin de Jong [79] and Drescher [80]. We show two typical photoelastic images that contrast states that have been achieve by isotropic compression and by shear in figure 7. In figure 8, we show a close-up of a single photoelastic particle that has three contacts. A disk that is subject to a set of point forces has a photoelastic pattern that uniquely represents the set of

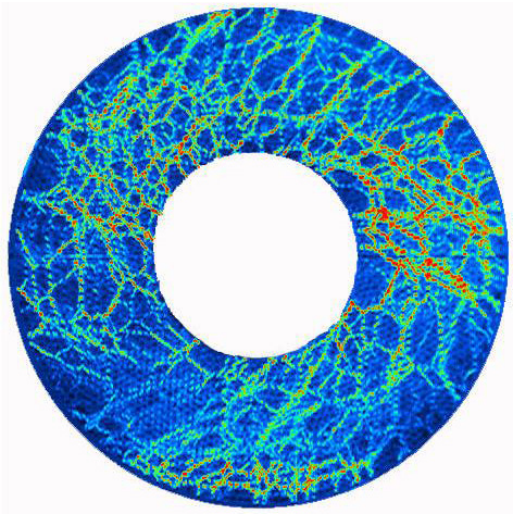

Figure 4. Image from experiments of Howell *et al* [20, 21, 65] showing the response of a system of photoelastic disks to shear. In a photoelastic image, particles that carry larger/weaker forces appear brighter/darker. In this image, bright/dark is mapped to color with bright/dark corresponding to red/blue. The experimental apparatus is a two dimensional Couette shear apparatus, where the inner boundary of an annulus rotates at a constant slow rate. Here, the rotation was clockwise, leading to force chains along the compressive shear direction (see below).

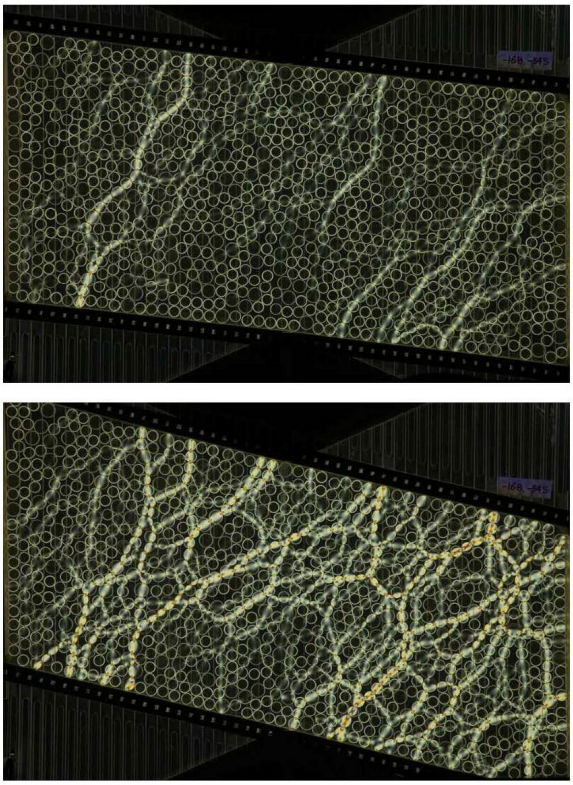

Figure 5. Fragile and shear jammed states, as seen in a simple shear experiment using photoelastic discs [39, 68]. In the experiment, discussed in more detail below, a rectangular container of discs is sheared quasi-statically from a rectangle to a parallelogram, without changing the area. The top image shows a fragile state for which the strong force network, i.e. the brighter discs, percolates from only in the compression direction. The bottom state shows a shear jammed state for which the strong network extends to all boundaries. (Note that a small portion of the actual experiment is not visible in these images.)

forces and their points of application. This property forms the basis of an inverse algorithm, first developed by Majmudar and Behringer [81], that determines quantitative vector inter-grain contact forces from photoelastic images of single particles. Figure 8 also shows more recent data from Zhang *et al* [82] that contrasts, clockwise from top left: an original color photoelastic image of a shear jammed state, a color filtered version of the same image that is the input to the force-inverse algorithm of Majmudar and Behringer [81], and Zhang *et al* [82], and a representation of the output of the algorithm giving the expected photoelastic image, based on the fitted contact forces and particle locations.

It is worth noting that the ability to obtain forces, contacts and other particle-scale data was crucial to understanding shear jamming [38, 81, 82], as discussed in section 4. Contact force data, in combination with the vector displacements between particles allows for the determination of the force moment tensor at the particle scale, and the full stress tensor at the system scale. Force data also makes it possible to map out strong and weak networks, or networks that exist above or below a chosen force normalization. These data also allow for the determination of statistical constructions such as force tiles [83], or contemplation of a detailed comparison at the smallest scales between an experiment and a numerical simulation [65, 84].

Empirically, a photoelastic image exhibits a series of light and dark fringes, and the pressure, or more properly, the trace of the particle scale force moment tensor acting on a particle is usually well approximated by computing the square gradient of the image intensity, averaged over a particle. This technique, which is computationally very efficient, was first used by Howell *et al* [14, 21, 65, 66], e.g. figures 4 and 9, and it provides force information at the particle scale in experiments. The key point is that using photoelastic particles with appropriate imaging and processing allows complete access to all mechanical properties of a system from the particle scale upwards.

Figure 9 shows particle-scale force distributions as a function of mean density, where Howell *et al* [14, 21] used the symbol γ for the packing fraction. These data pertain to a strongly anisotropic system, as characterized by figure 4. Notably, the mean force/particle vanishes at a packing fraction, $\phi_c = 0.766$. The force distributions for $\phi \geqslant 0.795$ show an exponential fall-off seen in similar situations [40, 42, 43], and a peak at low force. The data indicate a transition in the range $0.790 \leqslant \phi \leqslant 0.795$ where the exponential tail vanishes. As discussed below, this system exhibits a shear band, such that ϕ is lower near the inner boundary than in the rest of the system. This means that it is difficult to assign a single density for this system. The exponential tail of the force distribution has become a hallmark jammed granular systems, and recently, the behavior of the distribution below the peak has attracted attention in the context of yielding [85].

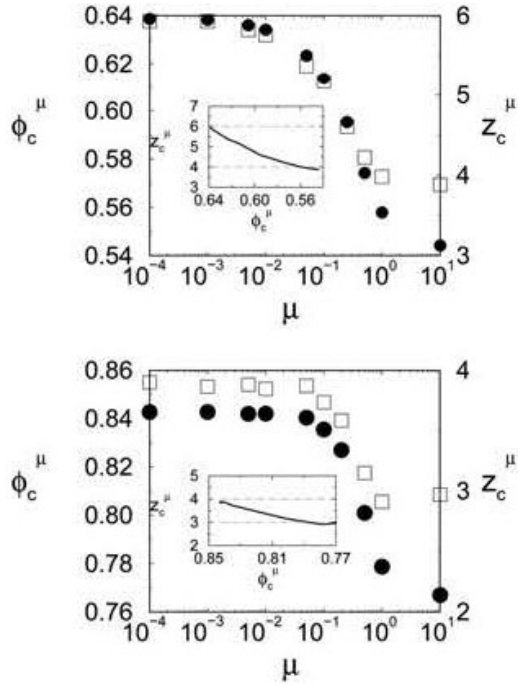

Figure 6. Data from Silbert [76] for values of ϕ and z at jamming for isotropic compression of systems of particles with a given friction coefficient, μ. Top: for spheres, Bottom for discs.

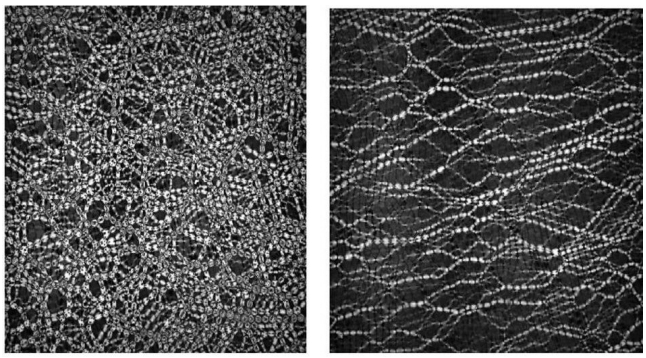

Figure 7. Photoelastic images from Majmudar and Behringer [81] contrasting an instropically compressed state and a shear jammed state.

3. Density-driven jamming and unjamming

In this section we review our understanding of the density-driven jamming transition, especially in frictionless grains, which necessarily comes from numerical simulations and the ensuing theoretical framework. The density-driven jamming transition of grains has been the subject of several reviews [5, 73], and here we only highlight the crucial features of this transition to set it in context of the range of jamming behavior observed in physical granular materials which have non-zero friction. We do not attempt or claim to do full justice to this field.

3.1. Hard sphere jamming

At zero temperature, hard spheres exist as a disordered solid (maximally random jammed state [86]) only at a the special

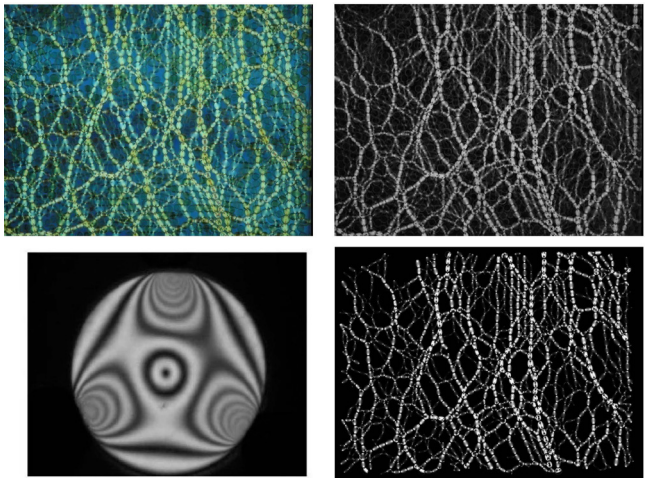

Figure 8. Photoelastic images. Clockwise from upper left: photoelastic image, as obtained with a high resolution color camera; this includes a raw photoelastic image, and a fitted image, plus a close-up of a single particle [82].

jamming point. Soft spheres can exist as disordered solids over a range of packing fractions and the unjamming point is the lower limit of stability of such solids [76, 87]. The unjamming transition is the solid-to-fluid transition of soft grains, and it has to do with both forces and positions. After all, strictly hard particles cannot be compressed beyond the jamming transition. There is a real physical boundary separating the allowed region in phase space of hard and soft grains. The jamming and the unjamming transitions could therefore hypothetically be defined by completely different physics. This is purely a consequence of granular assemblies being athermal. Introducing even an infinitesimal temperature eliminates this strict partitioning of phase space. Unjamming is concerned with the contact part of the stress tensor whose components vanish at the unjamming transition.

The hard-sphere jamming transition has been studied extensively in the last few years. Mean-field models [88–91] distinguish between the glass transition and the jamming transition. Other studies show that there is a well-defined maximally random jammed state [86] of hard particles, and that these disordered states are hyperuniform [92–95]: disordered solids with suppressed density fluctuations. Research from the group of Torquato, Stillinger and their collaborators have also provided us with valuable information about the influence of particle shape on the nature of jammed states, rigorous definitions of jamming and the notion of order parameters in jammed states [96].

3.2. Jamming and unjamming of soft spheres

The density-driven jamming and unjamming transitions of soft grains involve contact forces and stresses from the first term on the right side of equation (3). This feature clearly distinguishes the statistical framework that needs to be developed for soft grains from that of hard grains. For soft grains, jamming is the transition at which contact force networks are stabilized, and the jammed state is rigid to shear deformations. Therefore, this transition need not coincide with the

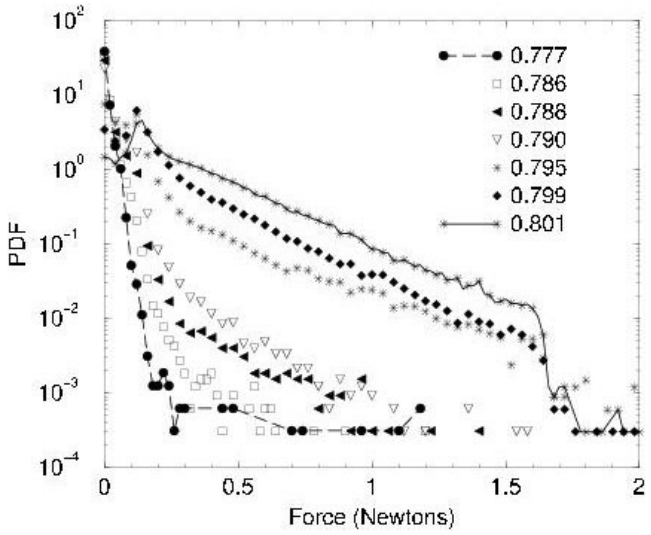

Figure 9. Distribution of the force, F acting on photoelastic particles for the ϕs indicated in the figure. These data, from Howell *et al* [20, 21, 65, 66], pertain to states that were created by steady-state quasi-static shear in a Couette geometry, as in figure 4. The forces were determined by using the G^2 method described below.

transition at which there are no solutions to the hard sphere packing problem. For a jammed state of soft spheres to be rigid, i.e. to have shear rigidity, nascent contact chains have to be stable under shear. Unjamming of frictionless soft grains, which has been extensively studied over the last two decades [44, 73] is characterized by the disappearance of mechanically stable solutions. This phenomenon can be described within the concept of isostaticity [30, 44] and the unjamming transition occurs at some protocol dependent density at which the structure becomes isostatic [75]. For spherical frictionless grains, it has been shown that the unjamming transition of soft grains occurs at the density at which hard spheres jam into the maximally random jammed state [44, 86].

The forces and stresses in frictionless systems are derivable from potentials: these are conservative systems. Therefore, jammed states sit at local minima of the potential energy. The questions of shear rigidity and mechanical stability can be referred to the properties of these minima [97]. The challenge in understanding frictionless jamming is understanding the role of the underlying disorder in the contact network [31], and classifying the enormously large number of local energy minima and their properties as an ensemble [98, 99]. From this perspective the jamming transition of frictionless grains and the glass transition share common features, and significant theoretical advances in understanding the jamming transitions have been made by extending meanfield approaches to the glass transition [88]. In contrast to jamming of frictional grains, jamming in frictionless systems can be completely characterized by the contact network and one does not need to analyze the force network as a separate entity. The constraints of mechanical equilibrium, however, do impose restrictions on the contact network in the jammed state even infinitesimally above the jamming transition. An important unanswered question in our view is the relationship between jammed contact networks and the networks defined by particles in near contact just below the jamming transition. Both networks are isostatic in the limit of $\phi \to \phi_J$ but it is not known whether distributions of microscopic variables characterizing the network are statistically similar. Below, we will discuss recent work that focuses on the statistical properties of jammed networks approaching the unjamming transition [31].

3.3. Force network ensemble

A framework for density-driven *unjamming* that has been developed for both frictionless and frictional grains is based on an assumption of scale separation between forces and grain-level compression. This assumption is justified for grains that are nearly rigid since a very small change in compression can lead to large changes in the contact forces. This framework, known as the force-network-ensemble [62, 100], assumes that all force balanced configurations on a given contact network are equally likely (Edwards equiprobability hypothesis). This approach has been used to study the distribution of contact forces in frictionless [100] and frictional [37] systems, to analyze the applicability of the Edwards stress ensemble, and also to explore the effects of body forces such as gravity on stress transmission [101].

3.4. Scaling at ϕ_J

The density-driven unjamming transition for frictionless particles is characterized by a special point with packing fraction ϕ_J and vanishing shear stress and temperature. This special point has many hallmarks of a classical critical point. Scaling analysis has established relationships between the exponents characterizing the power law behavior of physical properties approaching this transition from the jammed side [69, 70, 102–104]. This transition has been traditionally analyzed by characterizing the behavior of a few macroscopic quantities: pressure, average number of contacts, and bulk and shear moduli. In addition, it has been shown that the phonon spectra of frictionless jammed solids exhibit an excess of soft modes [97]. Growing length scales emerge at the unjamming transition, which have been associated with isostaticity [30, 71, 105, 106], and measured from the properties of the soft modes [71]. There are two such length scales characterized by different exponents [71]. The origin of these is not completely understood although recent scaling analysis sheds some light [69]. A different approach by Banigan *et al* to understanding the nature of the density-driven jamming transition in sheared systems has been based on the notion of chaotic dynamics [107]. In simulations, these authors find that jamming is associated with the onset of non-chaotic dynamics indicated by the vanishing of the first Lyapunov exponent, and the divergence of an associated dynamical length scale. This study suggests that jamming in slowly driven systems such as in the 2D Couette experiments of Howell *et al* [14, 21] is characterized by a growing dynamical length scale in contrast to the growing static length scaled identified at ϕ_J in frictionless unjamming of soft spheres.

The shear modulus and yield stress vanish continuously at the unjamming transition, and the former is described by a

power law with a non-trivial exponent. Pressure (from contact stresses) also vanishes at the unjamming transition as a power law with an exponent determined by the force law. A recent scaling description of jamming relates the exponents associated with the vanishing of bulk and shear moduli [69]. Recently, Muller and Wyart have argued that a jammed state created by a generic protocol has the characteristics of the marginal solid at the unjamming point [85]. And, recent experiments on emulsions by Brujic *et al* provide evidence for this marginal stability [3].

Recent work by Ramola and Chakraborty [108] has focused on the scaling properties of *distributions* of microscopic variables. This work demonstrates that distributions of areas covered by grains exhibit singularities at the unjamming transition, and that the macroscopic scaling laws can be derived from the scaling properties of these distributions.

3.5. Experiments

Majmudar *et al* [109] used a system of photoelastic particles to explore the concept of jamming in a physical granular material under isotropic conditions that were intended to provided a test of how well frictionless simulations by O'Hern *et al* [44] and later by Silbert *et al* [110] applied to systems of frictional particles. (At the time, there were no simulations of jamming in frictional systems.) The points of comparison for the simulations and these experiments, are z and P as functions of ϕ. It is not obvious that such experiments and the simulations should agree for several reasons. First, frictional particles are expected to have $z \simeq 3$ at jamming, compared to $z = 4$ for frictionless particles. Second, the algorithms used for the simulations sought a minimum energy as part of its calculation, whereas the frictional particles of the experiments did not have a conserved energy. Thirdly, the simulation algorithm 'grew' the particles uniformly, ensuring local isotropy; by contrast, in the experiments, the system was subject to compression or dilation from the boundaries. This is an example of a more general issue: various simulations and experiments often have different protocols for achieving what is thought to be a similar end state. But, the role of protocol is largely not understood. An additional part of the protocol for the experiments was that the particles rested on a smooth but still weakly frictional base that exerted a small drag on the particles that was not present in the simulations. However, the experimental protocol involved an additional step that tended to make the experiments more similar to the simulations: after each small strain step of compression/decompression, the system was gently 'tapped' to relax friction at contacts and friction with the base.

The experimental data by Majmudar *et al* [109] following the protocol above and shown in figure 10 substantively resemble the the frictionless simulations, although there were some residual differences. The expectations from the simulations are that z would be 0 below a certain ϕ_c, i.e. the jamming density, that it should then jump discontinuously to the isostatic value, $z = z_{\rm iso}$, and then grow as a power law in $\phi - \phi_c$ with an exponent of $\alpha = 1/2$. In fact, z for the experiments show a rapid increase over a small range of ϕ for a $\phi_c = 0.8422 \pm 0.0005$, followed by a continued increase as a power law with an exponent, $\alpha = 0.495$ if rattlers are included and $\alpha = 0.561$ if they are excluded. This is consistent with observations in simulations [44] and the theoretically predicted exponent of 1/2 based on isostaticity arguments [30]. Careful numerical studies, however, indicate corrections to these predictions, and a recent analysis [31] indicates $\alpha = 0.56$. Experiments on emulsions also measure an exponent closer to 0.56 [3]. The pressure in the Majmudar *et al* experiments increased above ϕ_c with an exponent of $\psi = 1.1 \pm 0.05$, which is consistent with predictions for frictionless particles and the measured interaction force law for the experimental particles. Recent work on scaling at the frictionless jamming transition [108] demonstrates how the exponents are determined by both the geometry of jammed packings and the force law.

The fact that z did not jump discontinuously at ϕ_c is not surprising. The determination of a contact has experimental error that substantially exceeds numerical simulations. Also, very weak contacts could be stabilized by the weak basal friction. This effect is presumably only relevant very close to jamming, and may contribute to the rounding of z versus ϕ.

Thus, there is reason to think that under the experimental protocol of Majmudar *et al* [109] the jamming of frictional particles is similar in character to jamming of frictionless particles, following the protocol of O'Hern *et al* [44]. We emphasize that if the relaxation part of the experimental protocol is omitted, the system jams at a much lower density.

3.6. Jamming in 3D experiments with visualization

Recent 3D compression experiments carried out by Brodu *et al* [111] showed that visualization at the grain scale, including contact forces and grain positions was possible. Specifically, these experiments consisted of uniaxial compression of hydrogel spheres in water. The friction coefficient for these spheres is very low, $\mu \simeq 10^{-2}$. Since the spheres were largely water in a polymer 'skeleton', they were only slightly denser than the water solution, and the uncompressed state was at nearly zero gravity. The lack of gravitational loading is important, since near-jamming systems are very soft, and small hydrostatic pressure can jam the system. The spheres also contained a fluorescent dye (Nile blue) that responded to laser excitation. When a laser sheet was swept across this system, the plane containing the laser sheet was bright where it intersected the spheres. An important part of this work was a set of algorithms that provided precise reconstruction of the particle surfaces. From this reconstruction, it was also possible to determine the deformation at contacts, and from that, the actual contact forces. Although laser scanning of granular systems was used previously [112], the important new feature of this work was the fact that it was possible to determine the inter-particle forces by determining the deformations at contacts. These experiments consisted of multiple cycles of uniaxial compression, starting from a state where the particles were just touching the top boundary which provided the compression. The pressure was a nonlinear function of strain,

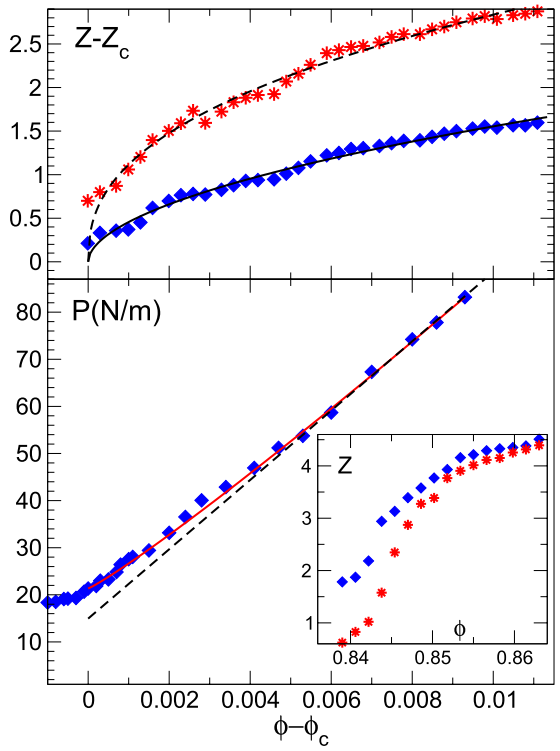

Figure 10. Data for the mean packing fraction, z and the system pressure versus $\phi - \phi_c$ (main figure) and versus ϕ (inset) from the experiments of Majmudar *et al* [109]. Near $\phi = 0.9845$, there is a significant jump in z. For $\phi > \phi_c$, there data for both z and P are consistent with power-laws in $\phi - \phi_c$, with exponents of $\sim$0.5 and $\sim$1.1 respectively.

and grew roughly as a power-law starting at $\phi = 0.62$, and continuing smoothly through $\phi = 0.64$ and up to values of $\phi \simeq 0.74$.

4. Shear-driven jamming

This section highlights the role of stress and stress response in jamming of physical granular materials where friction is important. One of the objectives is to clearly identify the roles played in jamming by two different but related networks: the contact network and the force network, which adds information about the magnitude and direction of the forces to the contact network. In frictionless systems with a well defined force law and only normal forces, the contact network carries all the information. By contrast, the hallmark of frictional granular materials is the indeterminacy of the forces, given only contact information. In the frictional case, the force and contact networks are necessarily distinct.

In the Liu–Nagel picture, jamming is driven by density and shear stress can only lead to unjamming. This is in contrast to the shear-driven rigidity picture of Cates *et al* [7]. Also, physical granular materials exhibit Reynolds dilatancy [113] in which a granular system expands under shear that is carried out under constant pressure. Thus, Reynolds dilatancy reflects physics similar to the Cates *et al* scenario, which pertains to shearing at fixed volume. Recent studies on frictional grains uncovered the phenomenon of shear jamming [38, 39, 82], which is a concrete realization of this theoretical scenario based on shear-driven solidification, [7] and is a conjugate phenomenon to Reynolds dilatancy.

Shear Jamming was discovered in experiments, as first reported by Bi *et al* [38] (see also Zhang *et al* [82] and Ren *et al* [39]). In these experiments, a 2D system of photoelastic disks is prepared in an initially stress-free state with a fixed density in the range $\phi_S < \phi < \phi_c$. When shear strain is applied, the system develops non-zero stresses and networks, or force chains, that evolve from fragile to robustly jammed with increasing shear strain, γ. The networks are highly anisotropic when they first form, and resemble the fragile states of Cates *et al* [7]. The particles that carry the majority of the force form force chains [19] that are roughly straight and that lie approximately along the compression direction of the applied shear.

Figure 11 shows the shear jamming phase diagram of Bi *et al* [38, 39, 82]. This figure is a sketch based on the experimental results shown in figure 13, as well as more recent data. It is slightly modified from the sketch of the original paper [38] to more accurately represent these experiments. The relevant theoretical framework has now been further developed [61, 64] to provide a quantitative characterization of shear jamming. Systems with packing fractions in the range $\phi_S < \phi < \phi_J$ where shear jamming occurs, can, for a given ϕ, have stress magnitudes ranging from zero to large values. Associated stresses and contact networks are often highly anisotropic and the force response of these states depends sensitively on the as-created, protocol dependent, force network. Two classes, depicted in the experimental images of figure 5, of states can be broadly identified in this packing fraction regime. Fragile states are created at low imposed stresses, have force-chains that percolate in the compressive direction [38] defined by the imposed shear stress, and can only resist compression along this direction. At higher stresses, there is a continuous transition to shear-jammed states characterized by force chains that percolate both in the compressive and dilational direction, and can support shear in both directions.

Several results from Bi *et al* [38] are key to characterizing shear jamming. These include identifying the formation of fragile and shear jammed states from the strong force networks, the identification of a clear onset of shear jammed states for a value of Z that is slightly above 3.0, and the observation that pressure, shear stress and Z all collapse onto common scaling curves, irrespective of the value of ϕ in the range $\phi_S < \phi < \phi_c$ when expressed in terms of the non-rattler fraction, $f_{\rm NR}$, as shown in figure 14, i.e. the fraction of particles that have at least two contacts. We show some of these results below. In figure 12, we show data for the length of the networks in the compression and dilation directions. The onset of fragile states occurs when the strong network first percolates in the compression direction. The system is shear jammed, i.e. able to resist strains in both compression and shear directions when the strong networks percolate in all directions. The results from many experiments to determine the onset of fragile and shear jammed states, figure 13, show several key features. As might be expected, there is a lowest $\phi = \phi_S$ below which shear jamming is not observed. But, more remarkably,

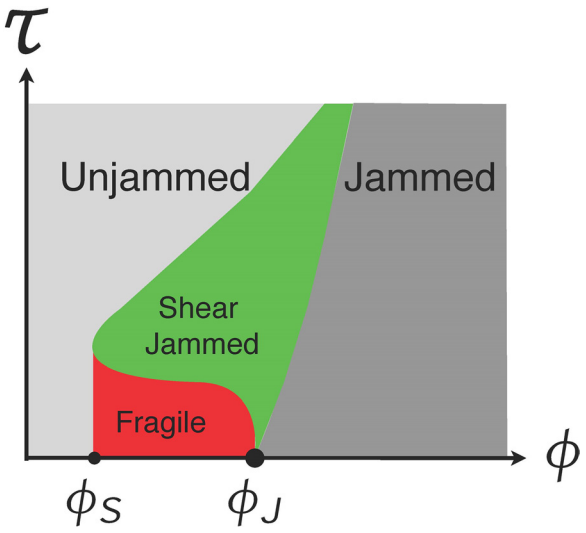

Figure 11. Shear jamming phase diagram for frictional granular materials, after Bi *et al* [38]. The dark gray region indicates states, characterized by τ and ϕ for which frictionless materials would be jammed. Frictional systems jam at lower ϕ, and in particular, there is a reentrant region. In $\phi_S < \phi < \phi_J$, systems with the same ϕ can be unjammed, fragile in the sense of Cates *et al* [7], or shear jammed. Fragile states are highly anisotropic, and only stable to one direction of shear strain. Shear jammed states are also anisotropic, but can resist both forward and reverse shear. For large enough τ, shear jammed states reach the yield stress curve, where the material will begin to flow.

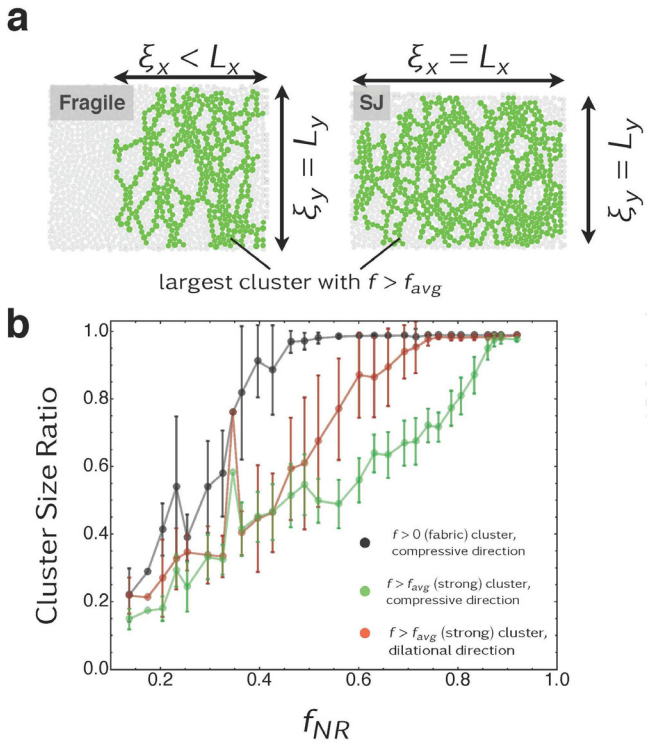

Figure 12. Fragile and percolating networks as seen in the pure shear experiments of Bi *et al* The compressive direction corresponds to y, and the dilation direction to x. In the fragile states of part (a), the strong force network percolates in the compressive direction, but not in the dilation direction. In the shear jammed states (SJ), right part of (a), the strong force network percolates in all direction. Part (b) shows the ratio of the largest cluster for the indicated sets of particles to the lengths, L_y and L_x of the system in the compressive and dilation directions, as functions of $f_{\rm NR}$.

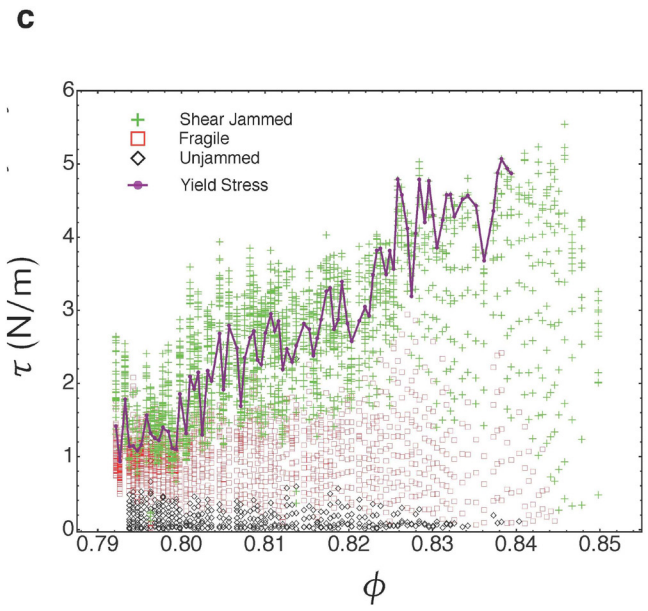

Figure 13. Experimental determination of shear jamming diagram, from Bi *et al* [38]. These data were obtained through multiple experiments at many different values of ϕ in the range of the figure. Each dot represents a state of the system, where black diamonds are unjammed states, red squares are fragile states, green crosses are shear jammed states, purple circles correspond to the yield stress surface.

there is a 'nose', i.e. a re-entrant part of the jamming diagram, indicating that there is a regime where unjammed, fragile and shear jammed states can all occur for the same ϕ. These data form the basis for the schematic jamming diagram, including shear jamming, in figure 11. $f_{\rm NR}$ is a monotonic but ϕ-dependent function of γ, as shown below.

The final feature of shear jamming from Bi *et al* that we reproduce here in figure 15, is data for the amount of shear strain needed to reach a shear jammed state. This quantity becomes large as $\phi \to \phi_S$ from above. The apparent limiting value of 0.79 suggested by this figure is likely larger than the true ϕ_S because the strain that could be attained in the experiments of Bi *et al* was modest.

Recent data by Wang *et al* [114] show that the strain needed to reach fragile and shear jammed states is also a function of friction. These data, figure 16, are for particles that are Teflon-wrapped and have low friction ($\mu \simeq 0.15$), moderate friction ($\mu \simeq 0.65$) 'bare' particles, and very high friction particles that have gear-like teeth along their surfaces.

One possible manifestation of shear jamming may be the formation of deep shear bands. For instance, the Howell *et al* experiments show a very deep shear band at the inner rotating surface of the Couette experiment, as in figure 17. The force networks, as in figure 4, cross the shear band without evident effect, despite the strong decrease in ϕ near the inner shearing surface. This is consistent with the re-entrant 'nose' of the shear jamming diagram: it is possible to have force-bearing states even at very low density. Except for a smooth radial dependence, the stresses in the mean, must be uniform from the inner to the outer surfaces of the experiment, reflecting overall force balance. This situation corresponds to a line

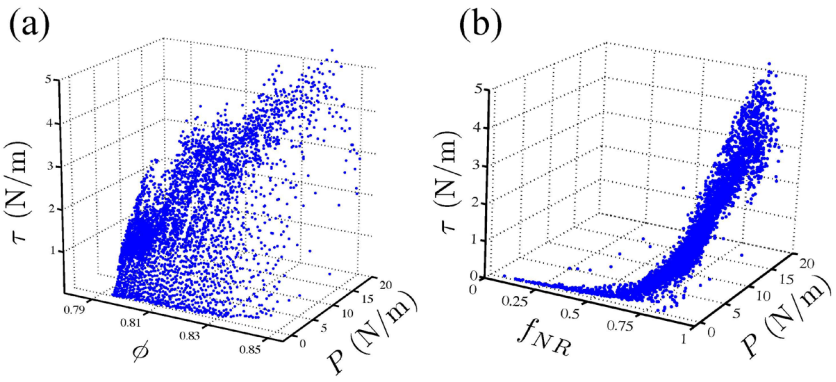

Figure 14. (a) Data for the pressure, P, and shear stress, τ, versus ϕ or versus $f_{\rm NR}$, the non-rattler fraction for many different experimental runs. (b) When these data are expressed in terms of $f_{\rm NR}$ instead of ϕ, the data collapse onto a common curve. Data from the experiments of Bi *et al* [38].

on the shear jamming diagram, figure 11, at roughly constant shear stress that starts at low ϕ near the nose of the shear jamming diagram, and extends towards the higher ϕ's that apply in the larger-radius parts of the system. Here, the notable point is that it is possible to have flowing, i.e. unjammed states for the low ϕ's in the shear band that resemble nearby static fragile states.

The onset of jamming by shear necessarily involves pressure, P, and shear stress, τ, that evolve with the strain, γ. P in particular grows nonlinearly with γ, as shown in figure 18 (Ren *et al* [39]). These data were obtained in a special apparatus that applies simple shear strain on the base as well as the boundaries of the system. This means that rattlers experience affine strain, and are not 'left behind'. This system does not form shear bands. Consequently, the system has uniform density, modulo small fluctuations, and exists in well defined states.

The data of figure 18 are consistent with the form

$$P(\phi) = (1/2)R(\phi)\gamma^2 \tag{4}$$

where the Reynolds coefficient, introduced by Ren *et al* [39], quantifies the strength of the nonlinear strain response. The growth of P with γ is a conjugate phenomenon to the usual Reynolds dilatancy, where a material that is sheared dilates against a weak confining stress. In the Ren *et al* experiments, the boundaries were rigid, prohibiting expansion, and leading instead to a strong increase in P. The Reyolds pressure observed by Ren *et al* implies that Reynolds dilatancy is an explicit part of shear jamming for particles with friction.

The dependence of R on γ, shown in figure 19 is also of interest. This quantity diverges strongly as $R = A(\phi_c - \phi)^\alpha$, where $\alpha = -3.3 \pm 0.1$, and $\phi_c = 0.84 \pm 0.004$, i.e. experimentally indistinguishable from $\phi_{\rm J}$ for isotropic jamming of frictionless particles.

Related experiments by Zheng *et al* [115] also involved shearing photoelastic discs in the shear jamming regime. But, in this case, the particles floated in a density-matched fluid, thus removing any effect from basal friction. In the Zheng *et al* experiments, P was zero up to some characteristic onset strain $\gamma_{\rm o}$ that depended on ϕ. As the strain was increased above $\gamma_{\rm o}$, P initially increased quadratically in $\gamma - \gamma_{\rm o}$ and then grew linearly for larger γ.

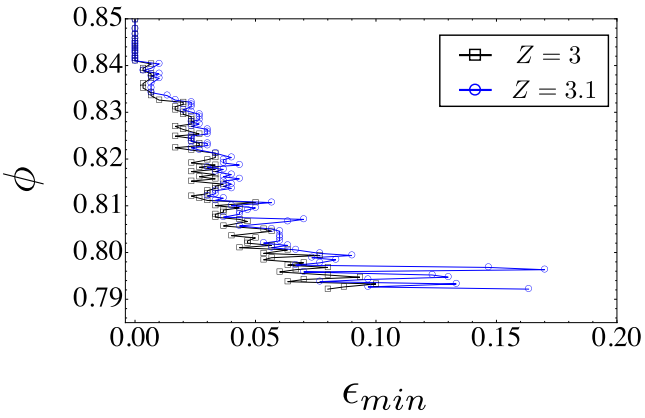

Figure 15. Minimum amount of shear strain needed for a given ϕ to reach a shear jammed state, after Bi *et al* [38]. Here, shear strain is represented by the symbol ϵ.

As with the data of Bi *et al* [38], the data of Ren *et al* [39, 68] collapse well when expressed as functions of the non-rattler fraction, $f_{\rm NR}$. Figures 20 and 21 show results for, respectively isotropic measures P and Z and anisotropic measures τ, fabric anisotropy, and stress anisotropy. The isotropic measures continue to grow over the full range of the experiments, whereas the anisotropic measures reach peaks and then decrease with $f_{\rm NR}$. The anisotropic behavior is a reflection of the fact that the force networks in the dilation direction lag those in the compression direction, but eventually 'catch up' with sufficient strain.

We also show in figure 22 the dependence of $f_{\rm NR}$ on γ for several different packing fractions. Necessarily, $f_{\rm NR}$ depends in an essential way on ϕ as well as γ, although it is possible to represent $f_{\rm NR}$ in a scaling form [83].

5. Experiments related to jamming

We consider additional experiments that inform the granular states near jamming. Early work by Rice, Bernal, Finney, Scott, and Kilgour focused on determining the densest and loosest packings that can be achieved by monodisperse (frictional) spheres that are randomly packed. In most cases, the spheres were subject to gravity, and in a mechanically stable

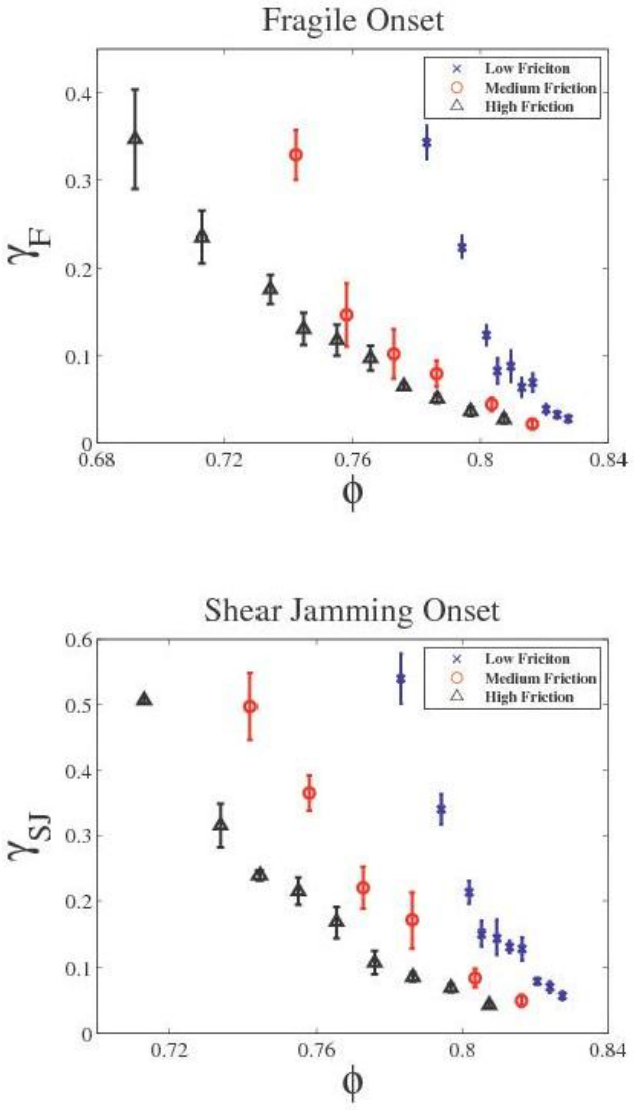

Figure 16. Minimum amount of shear strain to reach fragile and shear jammed states for various inter-particle friction coefficients, after Wang and Behringer [114].

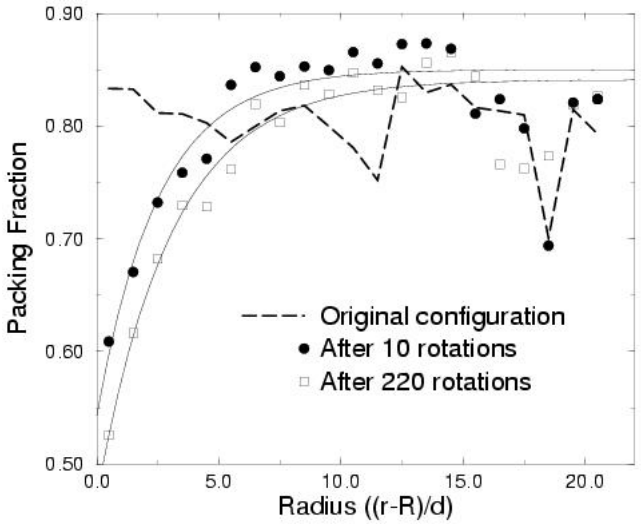

Figure 17. Data from the Couette shear experiment of Howell *et al* [20–22, 65] for the packing fraction profile as a function of the distance, expressed in units of the mean particle diameter, d, from the inner shearing wheel of the experiment. The original packing fraction profile, before the application of shear, is indicated by the dashed line. The solid circles and the open squares show the packing fraction profile after 10 and 220 rotations of the inner shearing wheel. A clear, and deep shear band forms as a result of the shear. The smooth lines are least-squares fits to a profile that decays exponentially with distance from the shear wheel to the large-radius value [22].

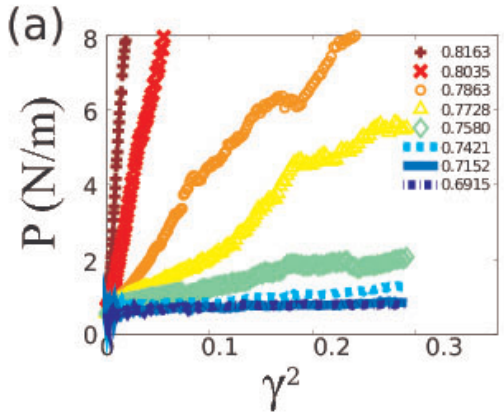

Figure 18. Pressure response versus γ^2 showing the nonlinear pressure response leading to shear jamming. The Reynolds coefficient, $(\partial^2 P/\partial\gamma^2)/2$ diverges strongly as ϕ approaches ϕ_J. Note that P grows (from 0) regardless of the direction of shear, hence the essential property that P is a nonlinear function of γ. (See also figure 19.)

state. Bernal [116] proposed packings of hard spheres as a model for fluids. A problem of particular interest was the range of packing fractions that could be achieved for random packings of spheres, typically confined in a container by gravity. Scott [117] and Scott and Kilgour [118] carried out detailed measurements using spheres made of steel, Plexiglas and Nylon. They used several different techniques to compact or dilate their samples, including simple pouring and tapping approaches that varied from manual tapping, to mechanical tapping, electromagnetic vibrators, air jets, and shearing. Scott [117] also measured and manipulated packing densities by placing particles in elastic balloons. These measurements took careful account of ordering and dilation effects at boundaries, and yielded maximum and minimum ϕ's (rcp and rlp, respectively) of 0.637 and 0.575. More recent experiments have extended these values a little bit, in particular the rlp density. (Note that the ϕ's corresponding to rlp and rcp are substantially lower than their counterparts in 2D.)

Onodo and Liniger [119] carried out a series of experiments that included sedimenting glass spheres into liquids with densities that could be almost as large as the bulk density from which the spheres were made. A key point was to observe the limit, as gravitational compaction vanished, for rlp. In this limit, they found $\phi = 0.555 \pm 0.005$. Onodo and Liniger also explored the extent of dilatancy as a function of ϕ using a Couette-type shear apparatus where the particle-fluid system was sheared between two cylinders. They found that dilatancy vanished at the rlp density. We note that dilatancy

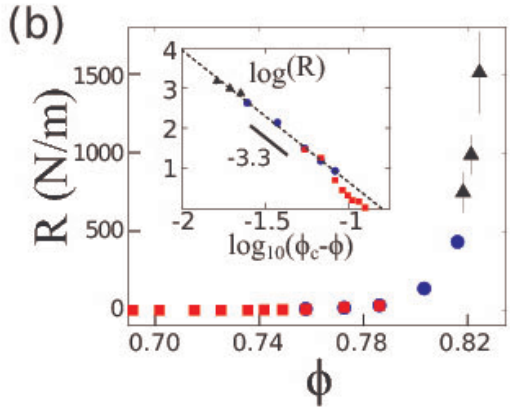

Figure 19. Reynolds coefficient $R = (\partial^2 P/\partial\gamma^2)/2$ versus ϕ from Ren *et al* [39]. These data reveal a diverging R that satisfies a power-law in $\phi_c - \phi$, where ϕ_c is experimentally indistinguishable from ϕ_J.

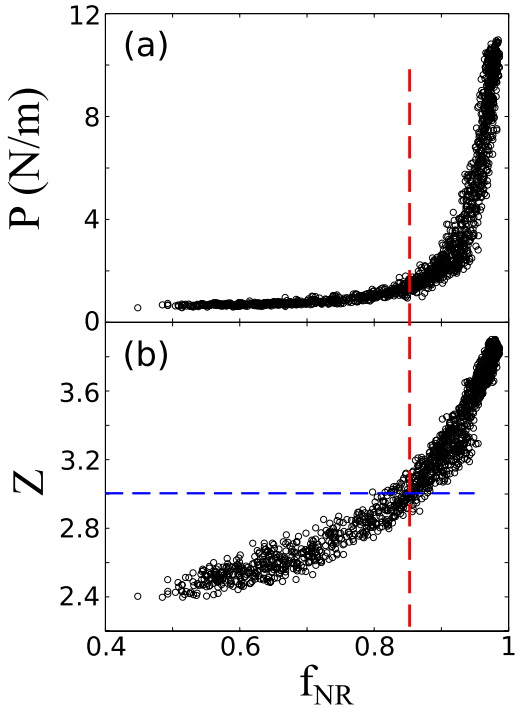

Figure 20. Scaling collapse of (a) P and (b) z as functions for the non-rattler fraction, f_{NR}, from the work of Ren *et al* [39, 68]. These results parallel those of Bi *et al* [38], for which a similar collapse is observed.

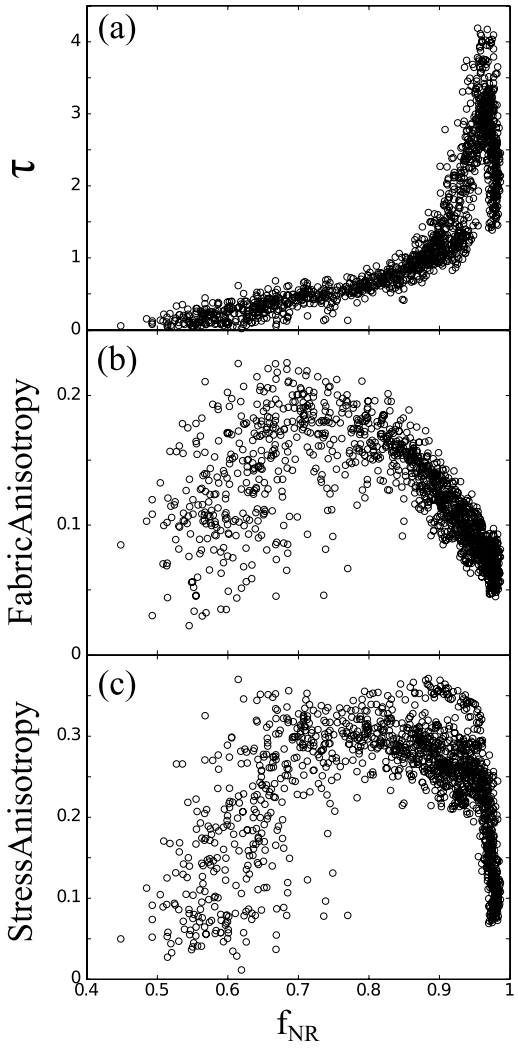

Figure 21. Scaling collapse versus f_{NR} for the shear stress, τ, the fabric anisotropy, given by the ratio of the difference to the sum of the fabric tensor eigenvalues, and the stress anisotropy, τ/P. These data correspond to five different ϕs in $\phi_S < \phi < \phi_J$. For small f_{NR}, there is significant scatter for some of these data, due to the sensitivity of the initial stress values to initial conditions, and to experimental errors which are relatively larger for smaller stresses and smaller values of f_{NR}.

is well known from soil mechanics, and was discovered by Reynolds [113]. If a material is not too loose, finite shear strain can only be accomplished if the material expands or dilates. This idea is incorporated into modern soil mechanics models, such as critical state soil mechanics [120].

The sedimentation approach was advanced with the development by Schroeter *et al* of fluidization techniques for a column of particles that are saturated with a fluid [121]. A pulse of fluidizing liquid lifts the column of particles, which then sediments under gravitational forces on the particles that are reduced by the buoyancy provided by the fluid. The final states are controlled by the length and strength of the fluidizing pulses, providing a fine control. The densities that can be achieved in any column experiment depend on how the gravitational forces are supported. If the fluid density is exactly matched to that of the grains, the particles are neutrally buoyant; in principle any ϕ up to rcp could be achieved. Otherwise, when the buoyancy is too low to support the full weight of the grains, there must be forces at the boundaries that support the residual load. This implies contact forces between the grains, and finite isotropic and shear stresses. The latter are typically non-zero, and can exert vertical forces on the walls. This is often explained in the context of a model due to Janssen [122] that assumes proportionality between vertical and horizontal stresses, and mobilization of friction at the sidewalls, leading to shear stress at the walls. Under these assumptions, the granular pressure as a function of distance from the top of the column decays exponentially to a limiting value, instead of increasing linearly with depth, as in a fluid.

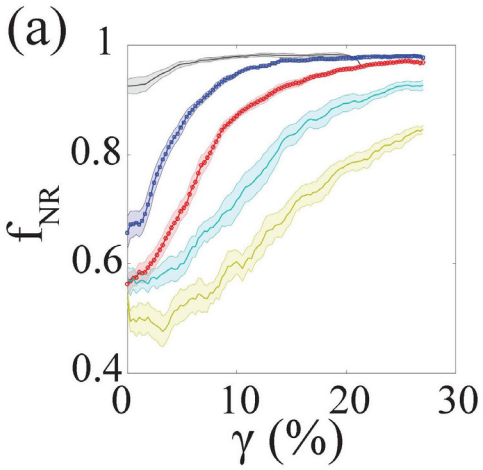

Figure 22. $f_{\rm NR}$ versus γ for five different values of ϕ, from the data of Ren *et al* [39]. (See also Sarkar *et al* [83].) The colors correspond to ϕ's according to gray: $\phi = 0.8269$; blue: $\phi = 0.8163$; red: $\phi = 0.8036$; cyan: $\phi = 0.7863$; yellow: $\phi = 0.7728$.

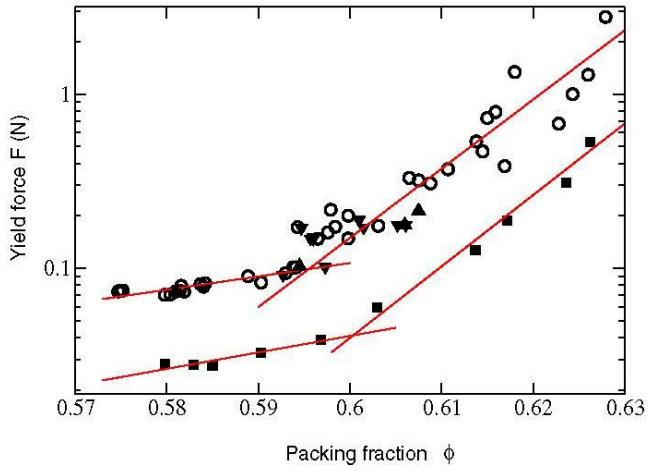

Figure 23. Data for the yield force as a function of ϕ for a rough plate (open circles and filled triangles) and a horizontal rod (solid squares) that are pulled from a carefully prepared system of glass spheres, after Métayer *et al* [126].

Jerkins *et al* [123] used fluidization of glass spheres with varying amounts of density matching to determine $\phi_{\rm rlp}$ in the limit of zero granular pressure, obtaining a value $\phi_{\rm rlp} = 0.550 \pm 0.001$. These authors found that this lowest value for $\phi_{\rm rlp}$ depended on the inter-particle friction coefficient: high friction led to operationally lower $\phi_{\rm rlp}$. In experiments by Farrell *et al* sequential deposition of cohesionless, monodisperse spherical particles whose frictional properties were very well characterized [124], shows a clearly decreasing trend of $\phi_{\rm rlp}$ with the static friction coefficient, μ. One of the distinguishing features of this experiment is that the particles are large enough to guarantee that they are outside the realm of attractive interactions. The results are consistent with the results, described above that were obtained with other protocols.

Schröter *et al* [125] and Métayer *et al* [126] considered the response of granular systems to respectively, the intrusion of a rod, and extraction of a rough plate, where the systems consisted of glass spheres that had been prepared over a range of densites using the fluidization method. The Schröter *et al* experiments extended earlier work by Schiffer *et al* [127, 128] and Hill *et al* [129], to allow for a range of system packing fractions. The Métayer studies yielded information on the shear response, again for a range of ϕ. Both studies found that responses that increased with increasing ϕ, and in particular, the ϕ-dependence of these responses was stronger above $\phi \simeq 0.595$, than below this value. Here, we highlight data from Métayer *et al* in figure 23 which show the yield force versus ϕ when pulling a rough plate (open circles and filled triangles), and when pulling a horizontal rod (solid squares).

The above work addresses the issue of a bulk property, the mean packing fractions for rlp and rcp packings. However, this does not elucidate the nature of structure associated with the packings, since there was no visualization. Schröder-Turk *et al* [130] used a variety of techniques, including fluidization, and tapping followed by x-ray computed tomography (CT) scans and numerical simulations, to prepare and characterize packings over the range of rlp to rcp. The goal was to develop an understanding of the extent of local packing anisotropy for states that are nominally globally isotropic. To characterize the local extent of anisotropy in the packing, these authors first computed the Voronoi tessilations of their samples, and then the Minkowski tensors for the Voronoi cells. They found strong anisotropy in the Voronoi cells, implying that the contact network at the local scale is similarly anisotropic. The average Voronoi anisotropy is characterized by parameters $\langle \beta_\nu^{rs} \rangle$, which are averages of eigenvalue ratios representing different aspects of anisotropy for a Voronoi volume. For spatially ordered packings, $\langle \beta_\nu^{rs} \rangle$ approaches 1, and it is lowest for rlp. Figure 24 shows some of their results. For all packings and for all $\langle \beta_\nu^{rs} \rangle$, there is a striking transition for $\phi = 0.64 = \phi_{\rm rcp}$. At the transition, the rate of change with ϕ of the $\langle \beta_\nu^{rs} \rangle$ changed sharply. The transition observed by Schröder-Turk *et al* is reminiscent of the sharp divergence in the Reynolds coefficient at the corresponding 2D rcp density observed by Ren *et al* [39].

In the work of Geng *et al* [131], a particle, the intruder, was pushed slowly and for large strains, through an annular channel filled with smaller photoelastic discs. The results from these experiments also demonstrate a density-related transition in the force response of granular systems. Primary data included the pushing force on the intruder and also the photoelastic response. These experiments showed a transition in the mean pushing force versus ϕ where the functional form of $\langle F \rangle$ changed discontinuously when $\phi \simeq 0.65$, figure 25. Below this density, the force response varied linearly with ϕ and above, it varied as $F \propto (\phi - \phi_t)^a$, where $a = 1.53$, indicating a more rapidly increasing (with ϕ) pushing force above the transition. (Geng *et al* used the symbol γ for the packing fraction.) These experiments can be contrasted to 3D studies by Albert *et al* [127, 132], who pushed rods through 3D systems of grains, and the work of Schröter *et al* [125] and Métayer [126] discussed above. In the Geng *et al* experiments, the system exists near the yield curve, and alternates between states that are stable, and states characterized by significant plastic deformation. The sharp functional change in

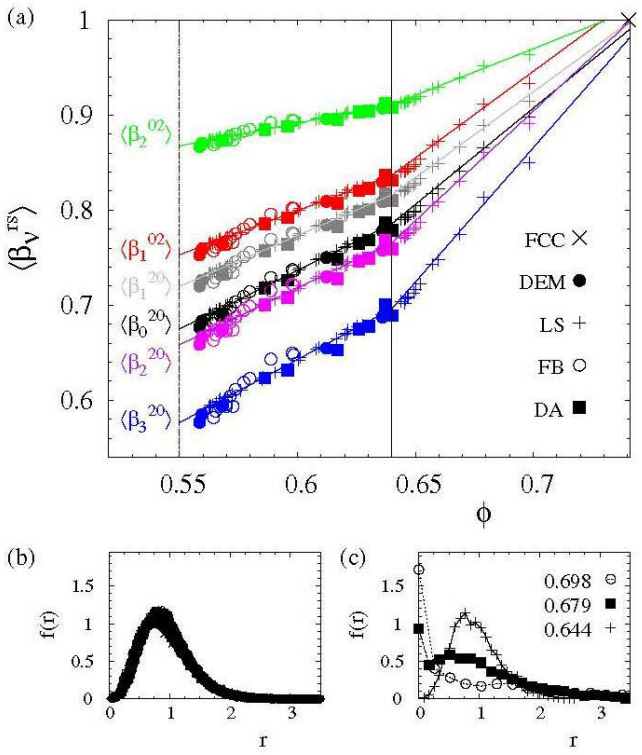

Figure 24. (a) Data for the means of the anistropy measures $\langle\beta_\nu^{rs}\rangle$ versus ϕ for Voronoi cells in 3D packings, after Schroeter-Turk, *et al* [130]. Isotropic packings have $\beta_\nu^{rs} = 1$. LS corresponds to data generated with the Lubachevsky–Stillinger algorighm, FB experimental data obtained by a fluidized bed method, and DA experimental data obtained with a tapping/compression method, (b) rescaled distributions for the anisotropy indices, $\langle\beta_\nu^{rs}\rangle$ versus $r = (1/\beta_\nu^{rs} - 1)/(1/\langle\beta_\nu^{rs}\rangle - 1)$ for experimental and simulated 3D packings having $0.55 < \phi < 0.64$ (c) similar results to those from (b) produced by the LS method, and at the packing fractions $\phi = 0.644$, $\phi = 0.679$, and $\phi = 0.698$. The peak at 0, grows with increasing ϕ and is indicative of semi-crystalline regions .

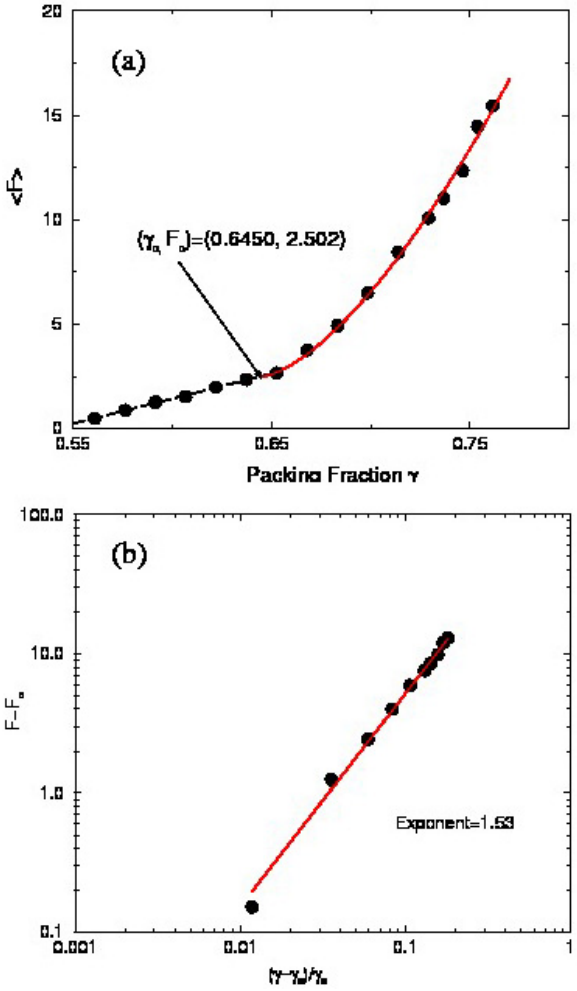

Figure 25. Data from Geng *et al* [131] for (a) the mean force $\langle F\rangle$ to quasi-statically push an intruder through a channel of 2D photoelastic particles versus the mean packing fraction, represented here by the symbol γ. In these data, $\langle F\rangle$ increases slowly with increasing γ, until there is a sharp change in slope, $d\langle F\rangle/d\gamma$. (b) F-F_c is plotted versus $(\gamma\text{-}\gamma_c)/\gamma_c$ to demonstrate the the scaling of <F> above the critical packing fraction γ_c, indicated in (a).

the average force at $\phi = 0.65$ suggests that for lower ϕ, the stable states are fragile, and for higher ϕ they are more robust, and hence shear jammed.

Related studies by Reichardt and Reichardt [133] involve pushing of a model intruder particle with a constant force through an assembly of frictionless discs interacting through a linear contact force law. These simulations differ from the Geng *et al* experiments in that the force law in the simulations is linear and frictionless, whereas the force law in the experiments is roughly Hertzian and the particles have friction. Also, the simulation protocol involves pushing the intruder at constant force, whereas the experiments involve pushing the intruder at constant speed. Nevertheless, these two studies show a number of similarities, including power-law dependencies of key quantities on the distance in density to jamming, and strong fluctuations in relevant quantities, e.g. intruder speed (simulations) and force on the intruder (experiments). For instance, both studies show a change in the intruder force dependence on ϕ at the onset of an appropriate jamming transition. In the simulations, the force needed to push the intruder through the system was zero below a jamming density of $\phi_J \simeq 0.84$, and was non-zero above that ϕ, i.e. the system exhibited a yield stress above ϕ_J. In the experiments, figure 25, the pushing force at constant speed increased linearly from $\phi \simeq 0.50$ to $\phi = 0.65$, and then increased faster with ϕ, for $\phi > 0.65$, as fragile force chain elements evolved.

In related studies, Candelier and Dauchot [134, 135] carried out experiments involving an intruder driven through a system of vibrated brass cylinders. Well below their observed ϕ_J, the intruder mean speed varied linearly with the pulling force, F, but on approach to ϕ_J from below, the intruder motion became intermittent, with $F \propto \ln(V)$. These authors reported ϕ_J that varied slightly from realization to realization. Near jamming, the intruder dynamics were intermittent, with bursts of displacement of length L and duration T. The distributions of T and F showed critical behavior exemplified by $P(T) = T^{-\alpha} f(T/\theta(\phi))$ where $\alpha \simeq 1/2$ and θ diverges as a power law in $\phi_J - \phi$.

6. Numerical studies and theoretical frameworks

In this section, we review numerical studies of jamming and the progress made in constructing a theoretical framework applicable to rigidity of and stress-transmission in jammed states.

6.1. Shear jamming in frictionless systems: numerical studies

Dilatancy and shear jamming in frictionless systems have been extensively studied in numerical simulations. As discussed earlier, Reynolds dilatancy occurs in granular systems when they are sheared under constant biaxial stress, which correspond to fixed pressure on one side, and uniaxial compression on the second, with fixed width in the third for three dimensional systems. There is emerging consensus that shear-jamming in *frictional* granular materials is a reflection of the consequences of dilatancy when granular materials are sheared under constant volume conditions. Note that biaxial strain always involves non-zero P, and hence has inherently different protocols and initial states than the shear jamming experiments. Under these conditions, shearing typically leads to increasing pressure, as discussed in 4.

The usual explanation of Reynolds dilatancy is based on a purely kinematic argument: hard particles have to expand to accommodate shear [113, 136]. The question of whether *frictionless* grains exhibit dilatancy is different. In a series of papers, Roux, Radjai and collaborators demonstrated that frictionless packings can support deviatoric stress but they do not exhibit dilatancy [136, 137] non-transiently. This observation then raises the question of whether frictionless grains exhibit Reynolds pressure, or shear-jamming under constant volume conditions.

Recent studies have addressed this question using numerical simulations. One important question that has been addressed is the behavior of these systems in the thermodynamic limit, i.e. as the number of particles diverges. Bertrand *et al* [138] and Baity-Jesi *et al* [139] have investigated the probability of creating jammed states with a finite value of the deviatoric stress as a function of packing fraction and systems size. Both of these studies show that in the thermodynamic limit, this probability becomes a step function at $\phi = \phi_J$. These studies are consistent with the Roux *et al* studies [136, 137] in that frictionless jammed packings can support deviatoric stress. In the thermodynamic limit, two types of jammed states can exist at ϕ_J: isotropic states with no deviatoric stress and anisotropic contact networks that support a deviatoric stress. Interestingly, Baity-Jesi *et al* [139] demonstrate that these two types of states have the same symmetry of the elastic modulus tensor: the states with deviatoric stress and the isotropic states differ only in the direction of the principal axis of the elastic modulus tensor. This observation was also made by Roux *et al* [136] for the systems that exhibited deviatoric stress but no dilatancy. Additional work by Luding *et al* [140, 141] and Vinutha and Sastry [142] are consistent with the Roux *et al* results, and the picture that has emerged is that shearing frictionless systems leads to a fabric of contacts that can exhibit pronounced anisotropy, and looks very similar to structures seen in frictional systems [142]. These structures can support a deviatoric stress. However, under shear, the force network undergoes constant rearrangement [136, 137]. In the constant pressure simulations [136, 137], the particles in the frictionless packings can have displacements in response to shear that lead to both dilation and compaction with no bias in either direction. This leads to the lack of macroscopic dilatancy. If friction biases the dilational displacements that can then explain Reynolds dilatancy.

In 3D constant volume studies, Vinutha and Sastry [142] have shown that the geometrical structures created by shearing frictionless systems below ϕ_J are mechanically unstable. They can be stabilized by introducing friction through a tangential spring. This observation is consistent with the lack of dilatancy in frictionless systems. It also suggests that the frictionless systems will not exhibit Reynolds pressure. Careful, precise studies of the Reynolds pressure in systems with different friction coefficients and increasing system sizes will be essential for understanding the difference between sheared states in frictional and frictionless systems. A lack of Reynolds pressure would imply the absence of shear jamming.

Interestingly, thermal hard spheres approaching the jamming transition, exhibit the phenomenon of Reynold's dilatancy [143]. Understanding the role of thermal fluctuations and friction on the phenomenon of Reynold's dilatancy will, in our view, help us gain better understanding of shear-jamming and even shear thickening in suspensions.

6.2. Ensembles of jammed states

As we have argued, in order to understand jammed states of frictional grains, we need to analyze both the contact network and the force network. The presence of large fluctuations and the underlying disorder in the contact network necessitates the use of statistical approaches in understanding the emergence of force networks in frictional granular media. Since the forces are not derivable from a potential, a microscopic jammed state is specified by both the set of positions and the set of contact forces. The contact forces are constrained to satisfy the requirements of mechanical equilibrium. In addition, contact vectors have to satisfy loop constraints since the grains form a packing in real space. A recent study has shown that one can solve this constraint satisfaction problem to obtain the contact forces from a knowledge of the contact network [144], thus opening up the possibility of analyzing properties of force networks in experiments that can only measure positions of grains, which includes the vast majority of studies. However, statistical theories of jamming and force transmission have to be based on a description of microstates that include grain positions and contact forces whether the latter are measured directly or obtained through the algorithm of [144]. In the next sections, we describe the construction of a theoretical framework that addresses the emergence of rigidity in dry, granular systems.

6.3. Constraints on granular aggregates: gauge potentials

The problem of rigidity of a dry granular packing can be formulated as a constraint satisfaction problem. Such a packing has to satisfy four different types of constraints which arise from the requirement of mechanical equilibrium at zero temperature. The constraints of force and torque balance have to be satisfied for every grain. Since the contacts are frictional, the Coulomb criterion of static equilibrium has to be satisfied. This introduces an additional constraint, $|f_t| \leqslant \mu f_n$, where μ is the coefficient of friction and $f_{t(n)}$ is the tangential (normal) component of the contact force. The interaction between dry grains is purely repulsive, hence the normal force always points towards the grain center, imposing a condition on the sign of the normal force, which by convention we phrase as an inequality constraint: $f_n \geqslant 0$. As discussed below, the constraints of force balance are the most straightforward to implement and can be incorporated in a geometric representation, dual to the real-space geometry. The inequality constraints and the torque balance constraint are not easily captured by this representation; however, they do play an important role in determining the statistical properties of the geometric patterns. There is also a global constraint that relates the sum of the grain level stresses to the external stresses imposed at the boundary.

The local nature of the constraints that need to be satisfied in a static granular packing allows a description of the system in terms of gauge potentials. A static granular aggregate is in mechanical equilibrium, and one of the necessary constraints is that the forces on every grain sum to zero: $\sum_c \vec{f}_{g,c} = 0$, where $\vec{f}_{g,c}$ represents the force acting on the grain g, through the contact c. The sum is taken over all the contacts $\{c\}$ for a given grain g. Newton's third law dictates that $\vec{f}_{g,c} = -\vec{f}_{g',c}$, at each contact c between the grains g and g'. These two constraints can be used to construct a representation of the forces in a granular packing known as the 'force tiling' representation [31, 61, 64, 145, 146], as illustrated in figure 26. In an alternative representation [16, 26, 147], the force at each contact can be written as: $\vec{f}_{g,c} = \vec{h}_v - \vec{h}_{v'}$, defining a set of height vectors $\{\vec{h}_v\}$, where g indexes a grain, c a contact, and v, v' index the two voids bracketing the contact $\{g, c\}$ (figure 27). Given a set of contact forces, the definition of $\{\vec{h}_{g,v}\}$ is unique, modulo a choice of origin: they are gauge potentials for the stress tensor, $\hat{\sigma}$ [16, 26]. From a continuum perspective, the height field can be viewed as the gauge potential that enforces $\nabla \cdot \hat{\sigma} = 0$

The force tiling and and height field representations are of course related: it is easy to see that the vertices of the force tiles represent the height vectors starting from an arbitrary origin since edges of the tiles represent the contact force vectors. The point pattern of these vertices provide information that is complementary to the positional pattern of grains. The bounding box enclosing the vertices is determined by the externally imposed stresses [61, 64]. Changing external *stresses* distorts the bounding box and can be viewed as the analog of 'strain' on the tilings, which leads to displacements of the vertices. The collective response of the vertices of the force tilings to this change is the analog of the response of particle positions to strain [61, 64]. This analogy has been used to construct a theory of shear-jamming that is discussed below.

6.4. Theories of shear jamming

Providing a theoretical basis that can characterize shear jamming is a subject of ongoing study. An approach taken in Sarkar *et al* [61, 64] is to analyze the *statistical* properties of the force tilings. Analysis of shear jamming and discontinuous shear thickening in suspensions show that the collective behavior of the tiles change across the transition. Ideas such as 'broken symmetry' that are crucial to understanding phase transitions have a counterpart in the force tilings. Measurements of order parameters and correlation functions in the space of tilings reveal clear signatures of shear jamming and shear thickening where real-space correlations fail to do so. Sarkar *et al* [61] has also used a representation of the local force states of grains in terms of a spin model. Depending on the region of parameter space, this model can capture the features of shear jamming, or the phenomenon of discontinuous shear thickening in sheared suspensions [148].

Since forces can be arbitrarily small, the heights are continuous variables. Any set of vertices in a force tile with N faces, and confined within the parallelogram bounded by $\left(\vec{F}_x, \vec{F}_y\right)$ represents a force-balanced configuration of N grains confined in a box of size $L_x \times L_y$, such that the integral of the stress tensor is:

$$\hat{\Sigma} = \begin{pmatrix} L_x & 0 \\ 0 & L_y \end{pmatrix} \times \begin{pmatrix} \vec{F}_x \cdot \hat{x} & \vec{F}_x \cdot \hat{y} \\ \vec{F}_y \cdot \hat{x} & \vec{F}_y \cdot \hat{y} \end{pmatrix}. \tag{5}$$

Thus, in the absence of any other constraints, the heights should not show any correlations. The torque balance condition, the positivity of the normal forces, and the Coulomb criterion, however, provide additional constraints that could lead to correlations between the vertices of the force tiles. The defining feature of a solid is its ability to resist shear: a consequence of breaking continuous translational symmetry [63]. Unlike a crystalline solid, defining an order parameter that signals this broken symmetry for disordered, amorphous solids is difficult [149] and is an outstanding problem. What is clear is that unlike a liquid, the patterns of particles persist in a solid. This persistence of patterns can be measured through an overlap order parameter that has been most widely used in spin glasses [150]. Figure 28 show a series of force tiles created from the set of experiments of Ren *et al* [39]. Shear jamming is captured by an overlap order parameter [61, 83] that measures the persistence of patterns of the vertices of force tiles at different strain steps (figure 29).

7. Looking beyond jamming

7.1. Applications and broader issues

Although the focus of this review is jamming of granular materials, we note that there are many broader issues associated with the science and application of particular matter. Here, we note of few of these, and we refer the reader to the extensive reviews in the review volume by Franklin and Shattuck [151].

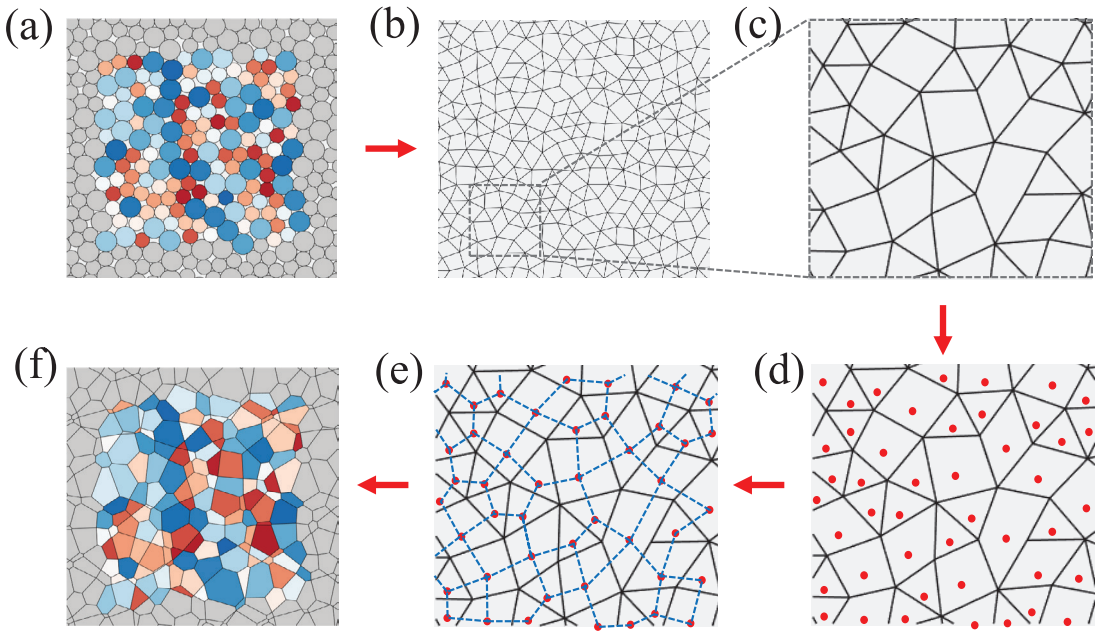

Figure 26. Illustration [83] of the mapping from positional space to force space: (a) a typical grain configuration. The colors are used to tag a grain and the corresponding force tile, otherwise they have no physical significance; (b) the real space contact network. (c) A portion of the real space contact network; (d) the faces (a point inside every face is marked by a red dot) of this portion of the real space contact network as obtained by constructing the minimum cycle basis; (e) the dual graph (blue dashed line) topology obtained from the minimum cycle basis. The edges of this dual graph become the edges of force tiles; (f) the force tiling for this configuration is obtained by distorting the dual graph according to the actual force vectors representing these edges. The force tiling is not a graph since the lengths and the angles between edges are meaningful quantities that carry information about the contact forces. The color of the force tile matches the color of the corresponding grain in (a).

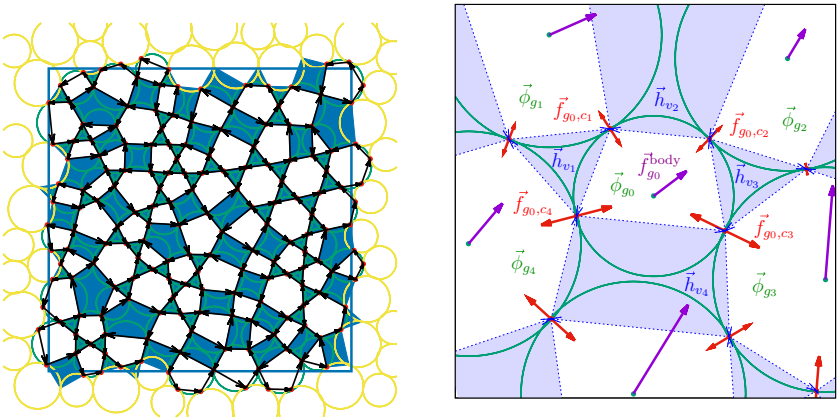

Figure 27. In two dimensional granular packings [16, 26, 147, 162], each contact is shared by two void polygons. (Left) Illustration of the partitioning into grain polygons (white) and void polygons (blue) for a jammed packing of 128 bidispersed frictionless disks. (Right) Enlarged view of a region of the packing on left showing location of height vectors and auxiliary fields ([162]).

7.1.1. Applications. Granular materials are of great practical as well as theoretical interest [152]. Examples of the former include soils, cereals, coal ores, sand and snow pharmaceutical powders, pills and feed stock for forming plastics. The cost of handling these materials is huge [153], and there is considerable need to have reliable and predictive tools for describing their flow and even static states for practical purposes.

7.1.2. Granular gases. In addition to jamming, which involves transtions between fluid-like and solid-like 'phases' granular materials have a gas-like phase. For instance, grains in a container with plenty of free space resemble a gas if they are shaken [154]. Although, arguably, granular gases are the best understood granular phase, the statistical mechanics of the gas state is still a subject of continued study. Granular gases exhibit novel phenomena, such as becoming inhomogeneous without continued energy input.

7.1.3. Force transmission in granular solids. A long-standing question regarding granular solids is how they respond to external stresses [6, 41]. This question is of considerable theoretical interest and it is crucial for many common engineering applications, such as the design of bins and hoppers. Highly evolved continuum models provide a practical tool [120]. But the nature of the differential equations on which they are based contain undesirable mathematical complexities,

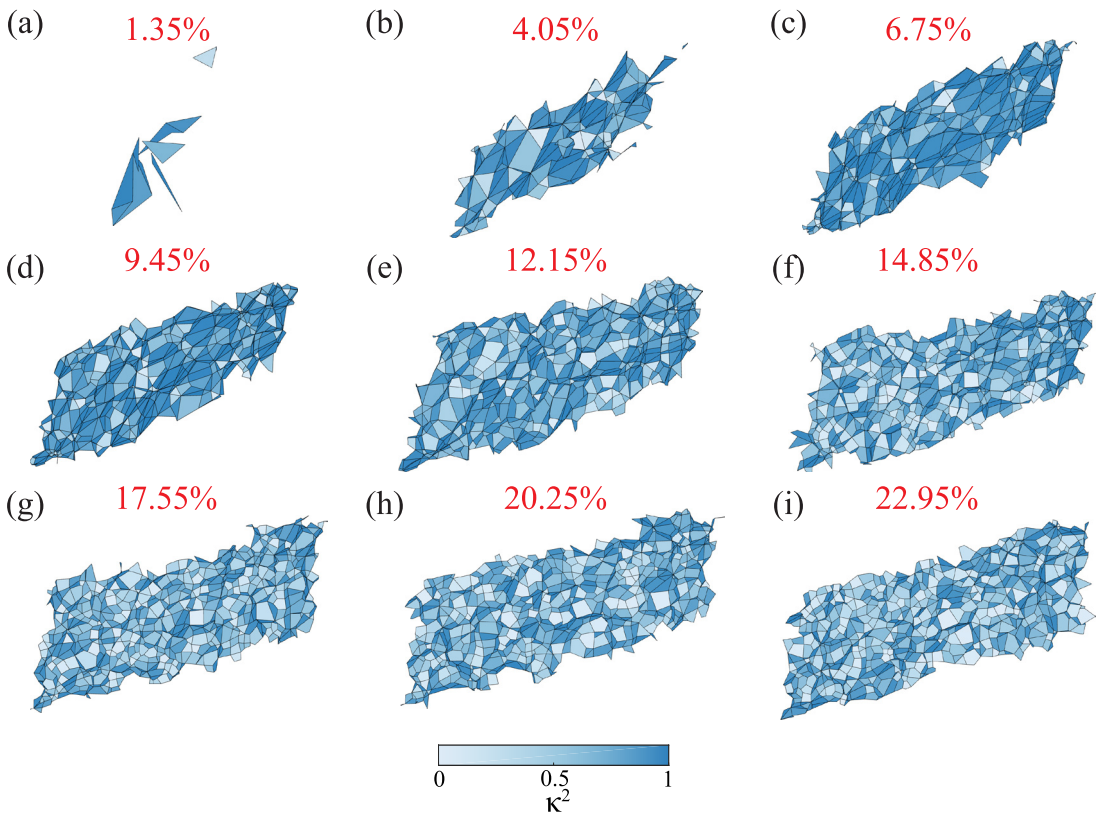

Figure 28. Force tiling: the evolution of the shape of the force tiles in a shear jamming experiment [39, 83] at $\phi = 0.8163$. For the sake of clarity, we have not shown the evolution of the size of the force tiles, which increases with increasing shear strain (marked on the snapshot). Each force tile is colored according to its asphericity, which provides a measure of how strong the tangential forces are in the system [83]. In the unjammed state (a), the force tiling is very small (due to small forces) and formless. In the fragile states ((b)–(d)) the force tilings are very anisotropic (as characterized by high asphericity of individual tiles) and begins as a quasi one dimensional structure (b), which evolves towards a well defined two dimensional shape as the shear jamming approaches (d). In the jammed states ((e)–(i)), the tiling has a well-defined shape which is preserved even when a large amount of strain is applied. Also, individual tiles become more isotropic.

including run-away instabilities [155–157]. At a more basic level, the question is: 'Is the force response of a granular solid to a small deformation elastic or is it described by some other model?' is at best partially answered, as reviewed in [41]. When materials are in a strongly jammed state, experiments and simulations indicate that an elastic description is likely reasonable [18, 45, 158–161]. However, when a system is a 'solid' but only slightly beyond jamming, then small perturbations can irreversibly deform or destabilize a system [8, 160].

A fundamental open question that has bearing on all the above aspects of stress transmission is how the constraints of *vector force balance* on a disordered network of contacts influence the response of granular systems to force perturbations.

Recent work [162] has focused on this question by extending the force-space representation discussed in section 6. To describe the response to a body force, the formalism was extended to include an additional set of gauge potentials, as described below. By introducing these auxiliary fields one can account for the change in the local stress tensor induced by an external perturbation. It was shown that the inhomogeneous propagation of stress through the system can be linked to the inherent randomness in the underlying fabric of contacts: the response of a granular packing to a localized force perturbation is related to the spectrum of the graph Laplacian representing the contact network of grains. These Laplacians form an ensemble of random matrices, and the stress transmission problem maps onto a problem of diffusion on a random network, which can lead to localized states [163].

The local constraints of mechanical equilibrium discussed in section 6 are also crucial in determining the response of jammed packings to external perturbations, and give rise to deviations from linear elasticity. In the presence of body forces, the continuum equation of mechanical equilibrium is $\nabla \cdot \hat{\sigma} = -\vec{f}_{\text{body}}$. We generalize the height field and force tiling framework, which impose mechanical equilibrium at the discrete grain level, to account for a localized body force by introducing additional *auxiliary fields on the grains* $\{\vec{\phi}\}$ (see figure 27). The sum of forces can then be represented as

$$\begin{aligned}
\vec{f}_{g_0,c_1} &= \vec{h}_{v_1} - \vec{h}_{v_2} + \vec{\phi}_{g_1} - \vec{\phi}_{g_0},\\
\vec{f}_{g_0,c_2} &= \vec{h}_{v_2} - \vec{h}_{v_3} + \vec{\phi}_{g_2} - \vec{\phi}_{g_0},\\
\vec{f}_{g_0,c_3} &= \vec{h}_{v_3} - \vec{h}_{v_4} + \vec{\phi}_{g_3} - \vec{\phi}_{g_0},\\
\underbrace{\vec{f}_{g_0,c_4}}_{-\vec{f}^{\text{body}}_{g_0}} &= \underbrace{\vec{h}_{v_4} - \vec{h}_{v_1}}_{0} + \underbrace{\vec{\phi}_{g_4} - \vec{\phi}_{g_0}}_{\Box^2\vec{\phi}_0}.
\end{aligned} \tag{6}$$

The summation on the right is simply the *network laplacian* defined, on grain g_0 as

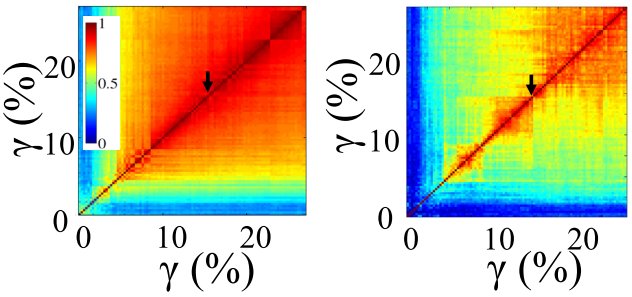

Figure 29. Map of the overlap matrix [61, 83] in strain (γ) space. (Left) Overlap of grain positions showing overlap $\approx$1 over the whole range. (Right) Overlap of height vertices showing the growth of high overlap regions with increasing strain. The arrows mark the onset of shear jamming [64].

$$\Box^2\vec{\phi}_0 = \vec{\phi}_{g_1} + \vec{\phi}_{g_2} + \vec{\phi}_{g_3} + \vec{\phi}_{g_4} - 4\vec{\phi}_{g_0}. \tag{7}$$

In general, one can write this equation in a vector notation as

$$\Box^2|\vec{\phi}\rangle = -|\vec{f}^{\text{body}}\rangle, \tag{8}$$

where $|\vec{\phi}\rangle$ represents the vector $(\vec{\phi}_1, \vec{\phi}_2, ...\vec{\phi}_N)$. We can *invert this equation* to obtain the auxiliary fields $\{\vec{\phi}\}$. Once we have determined the $\vec{\phi}$ field, we can construct force polygons for every grain and hence construct force tilings. This also means that we have determined effective contact forces that incorporate the effect of the body forces, and add up to zero on every grain. We can subtract $\Box\vec{\phi}$ from the original contact forces to obtain *effective contact forces* which satisfy the constraints of local force balance. The difference between these effective contact forces and the original ones represents the response of the granular packing to the perturbation.

7.1.4. Implications of shear jamming for rheology and for granular-like materials. As noted above, shear jamming is seen in the existence of random loose packings. But, there are other ways in which its effects are manifested, for instance in steadily sheared systems. The response of granular systems when they are steadily sheared is referred to as rheology, and is, by itself, a major research topic, and beyond the scope of this review. Using numerical simulations, Teitel *et al* [164], Heussinger *et al* [165], Otsuki and Hayakawa [166, 167] and others have extensively explored the states that occur for systems of frictionless and frictional particles that are subject to steady state shearing. Of particular interest here are studies by Otsuki and Hayakawa [166, 167] who explore the response of sheared systems of frictional particles near jamming, and contrast these to similar systems without friction. These studies show, among other things, that frictional systems exhibit a discontinuity in the shear stress and pressure as a function of ϕ, for the limit of vanishing shear rate. Steadily sheared systems are continuously rearranging, they are in some sense 'fluid-like'. An alternate analogy in this case is plastic yield in a solid. Many flows of practical interest fall in this category, and older granular models, such as critical state soil mechanics [120] provide continuum descriptions. More recently, there have been significant advances in understanding rheological flows using so-called $\mu(I)$ models [168]. The fact that sheared granular systems can statically or dynamically sustain shear bands, highly dilated regions within a granular material, is presumably related to shear jamming. And in simple shear flows, systems are close in density to shear jammed states. Then, when such a flow is arrested, as in a flow in a chute or hopper, the system can quickly transition from flowing to jammed, with an end state that is shear jammed. Thus, there are interesting connections to explore between granular rheology and shear jamming. And, it it is interesting to consider related phenomena occurring in systems such as suspensions or colloids.

For instance, in an interesting new development, analysis of recent experiments and numerical simulations in dense suspensions, which exhibit impact-driven solidification and the phenomenon of discontinuous shear thickening [148, 169–173], shows remarkable similarities with the phenomenon of shear jamming and the theoretical picture of stress transmission in shear-jammed solids that was presented in the 90's [7, 21]. There is a developing consensus that particle contact and friction play a crucial role in dense suspension rheology [174, 175]. Combining fluid mechanical interactions with contact friction between particles has been shown to capture critical features of both discontinuous shear thickening [148, 169, 172, 173, 176, 177] and shear induced jamming [178]. Furthermore, clear connections have been made between a dynamic shear-jamming front and impact-driven solidification [179]. The connection between shear-jamming in dry grains and shear-driven rigidity in dense suspensions is being actively explored but the field is too new for us to include in this review.

Acknowledgments

This research was supported by the WM Keck Foundation. The work of RPB was supported by NSF-DMR-1206351, NSF-DMS-1204871 and NASA grant NNX15AD38G. The work of BC was supported by NSF-CBET-1605428 and NSF-DMR-1409093. This research was also supported in part by the National Science Foundation under Grant No. NSF PHY11-25915. We acknowledge the hospitality of the Kavli Institute for Theoretical Physics where part of this work was carried out.

ORCID iDs

Robert P Behringer https://orcid.org/0000-0003-2499-2182
Bulbul Chakraborty https://orcid.org/0000-0002-3589-8207

References

[1] de Gennes P G 1999 Granular matter: a tentative view *Rev. Mod. Phys.* **71** S374–82
[2] Katgert G, Tighe B P and van Hecke M 2013 The jamming perspective on wet foams *Soft Matter* **9** 9739–46
[3] Lin J, Jorjadze I, Pontani L-L, Wyart M and Brujic J 2016 Evidence for marginal stability in emulsions *Phys. Rev. Lett.* **117** 208001

[4] Liu A and Nagel S 1998 Jamming is not just cool any more *Nature* **396** 21–2

[5] Liu A J and Nagel S R 2010 The jamming transition and the marginally jammed solid *Annu. Rev. Condens. Matter Phys.* **1** 347–69

[6] Bouchaud J-P 2002 Granular media: some ideas from statistical physics *Slow Relaxations and Nonequilibrium Dynamics in Condensed Matter Les Houches Session LXXVII* ed J-L Barrat *et al* (Berlin: Springer) pp 131–97

[7] Cates M E, Wittmer J P, Bouchaud J-P and Claudin P 1998 Jamming, force chains and fragile matter *Phys. Rev. Lett.* **81** 1841–4

[8] Schreck C F, Bertrand T, O'Hern C S and Shattuck M D 2011 Repulsive contact interactions make jammed particulate systems inherently nonharmonic *Phys. Rev. Lett.* **107** 078301

[9] Baxter G, Leone R, Johnson G and Behringer R 1991 Time-dependence, scaling and pattern-formation for flowing sand *Eur. J. Mech.* B **10** 181–6

[10] Miller B, O'Hern C and Behringer R 1996 Stress fluctuations for continuously sheared granular materials *Phys. Rev. Lett.* **77** 3110–3

[11] Goldhirsch I 2010 Stress, stress asymmetry and couple stress: from discrete particles to continuous fields *Granular Matter* **12** 239–52

[12] Zhang J, Behringer R P and Goldhirsch I 2010 Coarse-graining of a physical granular system *Prog. Theor. Phys. Suppl.* **184** 16–30

[13] Clark A, Mort P and Behringer R P 2012 Coarse graining for an impeller-driven mixer system *Granular Matter* **14** 283

[14] Veje C, Howell D W and Behringer R 1999 Kinematics of a two-dimensional granular couette experiment at the transition to shearing *Phys. Rev.* E **59** 739

[15] Maloney C E and Robbins M O 2008 Evolution of displacements and strains in sheared amorphous solids *J. Phys.: Condens. Matter* **20** 244128

[16] Ball R C and Blumenfeld R 2002 Stress field in granular systems: loop forces and potential formulation *Phys. Rev. Lett.* **88** 115505

[17] Edwards S and Oakeshott R 1989 Theory of powders *Physica* A **157** 1080–90

[18] Goldenberg C and Goldhirsch I 2004 Small and large scale granular statics *Granular Matter* **6** 87–96

[19] Radjai F, Jean M, Moreau J-J and Roux S 1996 Force distributions in dense two-dimensional granular systems *Phys. Rev. Lett.* **77** 274

[20] Howell D and Behringer R P 1997 Fluctuations and dynamics for a two-dimensional sheared granular material *Powders and Grains* ed R P Behringer and J T Jenkins (Leiden: A. A. Balkema) p 337

[21] Howell D, Behringer R and Veje C 1999 Stress fluctuations in a 2d granular couette experiment: a continuous transition *Phys. Rev. Lett.* **82** 5241

[22] Howell D W, Behringer R P and Veje C T 1999 Fluctuations in granular media *Chaos* **9** 559

[23] Blumenfeld R and Edwards S F 2009 On granular stress statistics: compactivity, angoricity and some open issues *J. Phys. Chem.* B **113** 3981–7

[24] Edwards S and Blumenfeld R 1994 *Granular Matter: An Interdisciplinary Approach* (Berlin: Springer)

[25] Baule A and Makse H A 2014 Fundamental challenges in packing problems: from spherical to non-spherical particles *Soft Matter* **10** 4423–9

[26] Henkes S and Chakraborty B 2009 Statistical mechanics framework for static granular matter *Phys. Rev.* E **79** 061301

[27] Bi D, Henkes S, Daniels K E and Chakraborty B 2015 The statistical physics of athermal materials *Annu. Rev. Condens. Matter Phys.* **6** 63–83

[28] Moukarzel C F 1998 Isostatic phase transition and instability in stiff granular materials *Phys. Rev. Lett.* **81** 1634–7

[29] Tkachenko A V and Witten T A 1999 Stress propagation through frictionless granular material *Phys. Rev.* E **60** 687–96

[30] Wyart M 2005 On the rigidity of amorphous solids *Ann. Phys. Fr.* **30** 1–96

[31] Ramola K and Chakraborty B 2016 Disordered contact networks in jammed packings of frictionless disks *J. Stat. Mech.* 114002

[32] Lubensky T C, Kane C L, Mao X, Souslov A and Sun K 2015 Phonons and elasticity in critically coordinated lattices *Rep. Prog. Phys.* **78** 073901

[33] Donev A, Connelly R, Stillinger F H and Torquato S 2007 Underconstrained jammed packings of nonspherical hard particles: ellipses and ellipsoids *Phys. Rev.* E **75** 051304

[34] Schreck C F, Mailman M, Chakraborty B and O'Hern C S 2012 Constraints and vibrations in static packings of ellipsoidal particles *Phys. Rev.* E **85** 061305

[35] Mailman M, Schreck C F, O'Hern C S and Chakraborty B 2009 Jamming in systems composed of frictionless ellipse-shaped particles *Phys. Rev. Lett.* **102** 255501

[36] Zeravcic Z, Xu N, Liu A J, Nagel S R and van Saarloos W 2009 Excitations of ellipsoid packings near jamming *Europhys. Lett.* **87** 26001

[37] Henkes S, van Hecke M and van Saarloos W 2010 Critical jamming of frictional grains in the generalized isostaticity picture *Europhys. Lett.* **90** 14003

[38] Bi D, Zhang J, Chakraborty B and Behringer R P 2011 Jamming by shear *Nature* **480** 355–8

[39] Ren J, Dijksman J A and Behringer R P 2013 Reynolds pressure and relaxation in a sheared granular system *Phys. Rev. Lett.* **110** 018302

[40] Makse H A, Johnson D L and Schwartz L M 2000 Packing of compressible granular materials *Phys. Rev. Lett.* **84** 4160

[41] Behringer R P 2016 Forces in static packings *Handbook of Granular Materials* ed S V Franklin and M D Shattuck (Boca Raton, FL: CRC Press) pp 249–84

[42] Coppersmith S, Liu C-H, Majumdar S, Narayan O and Witten T 1996 Model for force fluctuations in bead packs *Phys. Rev.* E **53** 4673

[43] Radjai F, Wolf D E, Jean M and Moreau J-J 1998 Bimodal character of stress transmission in granular packings *Phys. Rev. Lett.* **80** 61–4

[44] O'Hern C S, Silbert L E, Liu A J and Nagel S R 2003 Jamming at zero temperature and zero applied stress: the epitome of disorder *Phys. Rev.* E **68** 011306

[45] Geng J, Reydellet G, Clément É and Behringer R 2003 Green's function measurements of force transmission in 2d granular materials *Physica* D **182** 274–303

[46] Geng J, Howell D, Longhi E, Behringer R, Reydellet G, Vanel L, Clément E and Luding S 2001 Footprints in sand: the response of a granular material to local perturbations *Phys. Rev. Lett.* **87** 035506

[47] Vanel L, Howell D, Clark D, Behringer R and Clément E 1999 Memories in sand: experimental tests of construction history on stress distributions under sandpiles *Phys. Rev.* E **60** R5040

[48] Zhou J, Long S, Wang Q and Dinsmore A 2006 Measurement of forces inside a three-dimensional pile of frictionless droplets *Science* **312** 1631–3

[49] Ostojic S, Somfai E and Nienhuis B 2006 Scale invariance and universality of force networks in static granular matter *Nature* **439** 828–30

[50] Peters J F, Muthuswamy M, Wibowo J and Tordesillas A 2005 Characterization of force chains in granular material *Phys. Rev.* E **72** 041307

[51] Tordesillas A, Walker D M and Lin Q 2010 Force cycles and force chains *Phys. Rev.* E **81** 011302

[52] Goullet A, O'Hern C S, Kramar M, Mischaikow K and Behringer R P 2012 Topology of force networks in compressed granular media *Europhys. Lett.* **97** 54001

[53] Tordesillas A, Walker D M, Froyland G, Zhang J and Behringer R P 2012 Transition dynamics and magic-number-like behavior of frictional granular clusters *Phys. Rev.* E **86** 011306

[54] Bassett D S, Owens E T, Daniels K E and Porter M A 2012 Influence of network topology on sound propagation in granular materials *Phys. Rev.* E **86** 041306

[55] Kramar M, Goullet A, Kondic L and Mischaikow K 2013 Persistence of force networks in compressed granular media *Phys. Rev.* E **87** 042207

[56] Bassett D S, Owens E T, Porter M A, Manning M L and Daniels K 2015 Extraction of force-chain network architecture in granular materials using community detection *Soft Matter* **11** 2731–44

[57] Tordesillas A, Tobin S T, Cil M, Alshibli K and Behringer R P 2015 Network flow model of force transmission in unbonded and bonded granular media *Phys. Rev.* E **91** 062204

[58] Kovalcinova L, Goullet A and Kondic L 2016 Scaling properties of force networks for compressed particulate systems *Phys. Rev.* E **93** 042903

[59] Lim M X and Behringer R P 2017 Topology of force networks in granular media under impact *Europhys. Lett.* **129** 44003

[60] Takahashi T, Clark A H, Majmudar T and Kondic L 2018 Granular response to impact: topology of the force networks *Phys. Rev.* E **97** 012906

[61] Sarkar S, Bi D, Zhang J, Behringer R P and Chakraborty B 2013 Origin of rigidity in dry granular solids *Phys. Rev. Lett.* **111** 068301

[62] Tighe B P and Vlugt T J H 2011 Stress fluctuations in granular force networks *J. Stat. Mech.* P04002

[63] Chaikin P M and Lubensky T C 2000 *Principles of Condensed Matter Physics* (Cambridge: Cambridge University Press)

[64] Sarkar S and Chakraborty B 2015 Shear-induced rigidity in athermal materials: a unified statistical framework *Phys. Rev.* E **91** 042201

[65] Veje C T, Howell D W, Behringer R P, Scjöllmann S, Luding S and Herrmann H J 1998 Fluctuations and flow for granular shearing *Physics of Dry Granular Media* ed H J Herrmann *et al* (Dordrecht: Kluwer) p 237

[66] Howell D W 1999 Stress distributions and fluctuations in static and quasi-static granular systems *PhD Thesis* Duke University

[67] Chakraborty B and Behringer R P 2009 Jamming of granular matter *Encyclopedia of Complexity and Systems Science* ed R A Meyers (Berlin: Springer) p 4997

[68] Ren J 2013 Nonlinear dynamics and network properties in granular materials under shear *PhD Thesis* Duke University

[69] Goodrich C P, Liu A J and Sethna J P 2016 Scaling ansatz for the jamming transition *Proc. Natl Acad. Sci. USA* **113** 9745–50

[70] Goodrich C P, Dagois-Bohy S, Tighe B P, van Hecke M, Liu A J and Nagel S R 2014 Jamming in finite systems: stability, anisotropy, fluctuations and scaling *Phys. Rev.* E **90** 022138

[71] Silbert L E, Liu A J and Nagel S R 2005 Vibrations and diverging length scales near the unjamming transition *Phys. Rev. Lett.* **95** 098301

[72] Ikeda A, Berthier L and Sollich P 2012 Unified study of glass and jamming rheology in soft particle systems *Phys. Rev. Lett.* **109** 018301

[73] Van Hecke M 2010 Jamming of soft particles: geometry, mechanics, scaling and isostaticity *J. Phys.: Condens. Matter* **22** 033101

[74] Olsson P and Teitel S 2013 Athermal jamming versus thermalized glassiness in sheared frictionless particles *Phys. Rev.* E **88** 010301

[75] Chaudhuri P, Berthier L and Sastry S 2010 Jamming transitions in amorphous packings of frictionless spheres occur over a continuous range of volume fractions *Phys. Rev. Lett.* **104** 165701

[76] Silbert L E 2010 Jamming of frictional spheres and random loose packing *Soft Matter* **6** 2918–24

[77] Wakabayashi T 1950 Photo-elastic method for determination of stress in powdered mass *J. Phys. Soc. Japan* **5** 383–5

[78] Dantu P 1957 Contribution à l'étude mécanique et géométrique des milieux pulvérulents *Proc. of the 4th Int. Conf. on Soil Mechanics and Foundation Engineering (London)* vol 1 (Butterworths Scientific Publications) pp 144–8

[79] Drescher A and de Josselin G 1972 Photoelastic verification of a mechanical model for the flow of a granular material *J. Mech. Phys. Solids* **20** 337–51

[80] Drescher A 1976 An experimental investigation of flow rules for granular materials using optically sensitive glass particles *Géotechnique* **26** 591–601

[81] Majmudar T S and Behringer R P 2005 Contact force measurements and stress-induced anisotropy in granular materials *Nature* **435** 1079–82

[82] Zhang J, Majmudar T, Tordesillas A and Behringer R 2010 Statistical properties of a 2d granular material subjected to cyclic shear *Granular Matter* **12** 159–72

[83] Sarkar S, Bi D, Zhang J, Ren J, Behringer R P and Chakraborty B 2016 Shear-induced rigidity of frictional particles: analysis of emergent order in stress space *Phys. Rev.* E **93** 042901

[84] Dijksman J, Kovalcinova L, Ren J, Behringer R, Kramer M, Mischaikow K and Kondic L 2018 Characterizing granular networks using topological metrics (arXiv: 1801.03060)

[85] Müller M and Wyart M 2015 Marginal stability in structural, spin and electron glasses *Annu. Rev. Condens. Matter Phys.* **6** 177–200

[86] Torquato S, Truskett T and Debenedetti P 2000 Is random close packing of spheres well defined? *Phys. Rev. Lett.* **84** 2064–7

[87] Kumar N and Luding S 2016 Memory of jamming—multiscale models for soft and granular materials *Granular Matter* **18** 58–80

[88] Charbonneau P, Kurchan J, Parisi G, Urbani P and Zamponi F 2014 Fractal free energy landscapes in structural glasses *Nat. Commun.* **5** 3725

[89] Charbonneau P, Corwin E I, Parisi G and Zamponi F 2012 Universal microstructure and mechanical stability of jammed packings *Phys. Rev. Lett.* **109** 205501

[90] Charbonneau P, Ikeda A, Parisi G and Zamponi F 2011 Glass transition and random close packing above three dimensions *Phys. Rev. Lett.* **107** 185702

[91] Parisi G and Zamponi F 2010 Mean-field theory of hard sphere glasses and jamming *Rev. Mod. Phys.* **82** 789

[92] Wu Y, Olsson P and Teitel S 2015 Search for hyperuniformity in mechanically stable packings of frictionless disks above jamming *Phys. Rev.* E **92** 052206

[93] Donev A, Stillinger F and Torquato S 2005 Unexpected density fluctuations in jammed disordered sphere packings *Phys. Rev. Lett.* **95** 090604

[94] Uche O, Stillinger F and Torquato S 2004 Constraints on collective density variables: two dimensions *Phys. Rev.* E **70** 046122

[95] Torquato S and Stillinger F 2003 Local density fluctuations, hyperuniformity and order metrics *Phys. Rev.* E **68** 041113

[96] Kansal A R, Torquato S and Stillinger F H 2002 Diversity of order and densities in jammed hard-particle packings *Phys. Rev.* E **66** 041109

[97] Wyart M, Nagel S R and Witten T 2005 Geometric origin of excess low-frequency vibrational modes in weakly connected amorphous solids *Europhys. Lett.* **72** 486

[98] Martiniani S, Schrenk K J, Ramola K, Chakraborty B and Frenkel D 2017 Numerical test of the Edwards conjecture shows that all packings are equally probable at jamming *Nat. Phys.* **13** 848

[99] Martiniani S, Schrenk K J, Stevenson J D, Wales D J and Frenkel D 2016 Turning intractable counting into sampling: computing the configurational entropy of three-dimensional jammed packings *Phys. Rev.* E **93** 012906

[100] Snoeijer J H, Vlugt T J, van Hecke M and van Saarloos W 2004 Force network ensemble: a new approach to static granular matter *Phys. Rev. Lett.* **92** 054302

[101] Tighe B P, Nakagawa M and Luding S 2009 Granular lattice models with gravity *AIP Conf. Proc.* **1145** 305–8

[102] Olsson P and Teitel S 2012 Herschel-bulkley shearing rheology near the athermal jamming transition *Phys. Rev. Lett.* **109** 108001

[103] Olsson P and Teitel S 2011 Critical scaling of shearing rheology at the jamming transition of soft-core frictionless disks *Phys. Rev.* E **83** 030302

[104] Vågberg D, Olsson P and Teitel S 2011 Glassiness, rigidity and jamming of frictionless soft core disks *Phys. Rev.* E **83** 031307

[105] Mailman M and Chakraborty B 2012 *J. Stat. Mech.* P05001

[106] Mailman M and Chakraborty B 2011 *J. Stat. Mech.* L07002

[107] Banigan E J, Illich M K, Stace-Naughton D J and Egolf D A 2013 The chaotic dynamics of jamming *Nat. Phys.* **9** 288

[108] Ramola K and Chakraborty B 2017 Scaling theory for the frictionless unjamming transition *Phys. Rev. Lett.* **118** 138001

[109] Majmudar T, Sperl M, Luding S and Behringer R P 2007 Jamming transition in granular systems *Phys. Rev. Lett.* **98** 058001

[110] Silbert L E, Liu A J and Nagel S R 2006 Structural signatures of the unjamming transition at zero temperature *Phys. Rev.* E **73** 041304

[111] Brodu N, Dijksman J A and Behringe R P 2015 Spanning the scales of granular materials: microscopic force imaging *Nat. Commun.* **6** 6361

[112] Dijksman J A, Brodu N and Behringer R P 2017 Refractive index matched scanning and detection of soft particles *Rev. Sci. Instrum.* **88** 051807

[113] Reynolds O 1885 On the dilatancy of media composed of rigid particles in contact, with experimental illustrations *Phil. Mag. Ser.* **50** 469–81

[114] Wang D and Behringer R P 2017 Effect of friction on shear jamming preprint

[115] Zheng H, Dijksman J A and Behringer R P 2014 Shear jamming in granular experiments without basal friction *Europhys. Lett.* **107** 34005

[116] Bernal J D 1987 Concluding remarks *Proc. R. Soc.* A **280** 299–322

[117] Scott G D 1960 Packing of spheres: packing of equal spheres *Nature* **188** 908–9

[118] Scott G and Kilgour D M 1969 The density of random close packing of spheres *Br. J. Appl. Phys. (J. Phys. D)* **2** 863–6

[119] Onodo G Y and Liniger E G 1990 Random loose packings of uniform spheres and the dilatancy onset *Phys. Rev. Lett.* **2** 2727–30

[120] Nedderman R M 1992 *Statics and Kinematics of Granular Materials* (Cambridge: Cambridge University Press) https://doi.org/10.1017/CBO9780511600043

[121] Schröter M, Nägle S, Radin C and Swinney H 2005 Phase transition in a static granular system *Europhys. Lett.* **71** 44004

[122] Janssen H A 1895 Versuche über getreidedruck in silozellen *Z. Vereines Deutscher Ingenieure* **39** 1045–9

[123] Jerkins M, Schröter M, Swinney H L, Senden T J, Saadatfar M and Aste T 2008 Onset of mechanical stability in random packings of frictional spheres *Phys. Rev. Lett.* **101** 018301

[124] Farrell G R, Martini K M and Menon N 2010 Loose packings of frictional spheres *Soft Matter* 2925–30

[125] Schröter M, Goldman D and Swinney H 2005 Stationary state volume fluctuations in a granular medium *Phys. Rev.* E **71** 030301R

[126] Métayer J-F, Suntrup D J III, Radin C, Swinney H L and Schröter M 2011 Shearing of frictional sphere packings *Europhys. Lett.* **93** 64003

[127] Albert I, Sample J, Morss A, Rajagopalan S, Barabási A-L and Schiffer P 2001 Granular drag on a discrete object: shape effects on jamming *Phys. Rev.* E **64** 061303

[128] Stone M B, Bernstein B R, Barry R, Pelc M D, Tsui Y K and Schiffer P 2004 Stress propagation: getting to the bottom of a granular medium *Nature* **427** 503–4

[129] Yeung G H S and Koehler S A 2005 Scaling vertical drag forces in granular media *Europhys. Lett.* **72** 137

[130] Schröder-Turk G E, Mickel W, Schröter M, Delaney G W, Saadatfar M, Senden T J, Mecke K and Aste T 2010 Disordered spherical bead packs are anisotropic *Europhys. Lett.* **90** 34001

[131] Geng J and Behringer R P 2005 Slow drag in two-dimensional granular media *Phys. Rev.* E **71** 011302

[132] Albert I, Tegzes P, Kahng B, Albert R, Sample J, Pfeifer M, Barabasi A-L, Vicsek T and Schiffer P 2000 Jamming and fluctuations in granular drag *Phys. Rev. Lett.* **84** 5122

[133] Reichardt C J O and Reichardt C 2010 Fluctuations, jamming and yielding for a driven probe particle in disordered disk assemblies *Phys. Rev.* E **82** 051306

[134] Candelier R and Dauchot O 2009 Creep motion of an intruder within a granular glass close to jamming *Phys. Rev. Lett.* **103** 128001

[135] Candelier R and Dauchot O 2010 Journey of an intruder through the fouidization and jamming transitions of a dense granular media *Phys. Rev.* E **81** 011304

[136] Peyneau P E and Roux J N 2008 Frictionless bead packs have macroscopic friction, but no dilatancy *Phys. Rev.* E **78** 011307

[137] Azéma É, Radja F and Roux J-N 2015 Internal friction and absence of dilatancy of packings of frictionless polygons *Phys. Rev.* E **91** 010202

[138] Bertrand T, Behringer R P, Chakraborty B, Shattuck M D and O'Hern C S 2015 Protocol dependence of the jamming transition *Phys. Rev.* E **93** 012901

[139] Baity-Jesi M, Goodrich C P, Liu A J, Nagel S R and Sethna J P 2017 Emergent so(3) symmetry of the frictionless shear jamming transition *J. Stat. Phys.* **167** 735–48

[140] Kumar N, Imole O I, Magnanimo V and Luding S 2014 Effects of polydispersity on the micro–macro behavior of granular assemblies under different deformation paths *Particuology* **12** 64–79

[141] Imole O I, Kumar N, Magnanimo V and Luding S 2013 Hydrostatic and shear behavior of frictionless granular assemblies under different deformation conditions *KONA Powder Part. J.* **30** 84–108

[142] Vinutha H and Sastry S 2016 Disentangling the role of structure and friction in shear jamming *Nat. Phys.* **12** 578–83

[143] Rainone C, Urbani P, Yoshino H and Zamponi F 2015 Following the evolution of hard sphere glasses in infinite dimensions under external perturbations: compression and shear strain *Phys. Rev. Lett.* **114** 015701
[144] Gendelman O, Pollack Y G, Procaccia I, Sengupta S and Zylberg J 2016 What determines the static force chains in stressed granular media? *Phys. Rev. Lett.* **116** 078001
[145] Maxwell J C 1890 *The Scientific Papers of James Clerk Maxwell* (New York: Dover)
[146] Tighe B P, van Eerd A R and Vlugt T J 2008 Entropy maximization in the force network ensemble for granular solids *Phys. Rev. Lett.* **100** 238001
[147] DeGiuli E 2012 Continuum limits of granular systems *PhD Thesis* University of British Columbia
[148] Mari R, Seto R, Morris J F and Denn M M 2014 Shear thickening, frictionless and frictional rheologies in non-Brownian suspensions *J. Rheol.* **58** 1693–724
[149] Kurchan J and Levine D 2011 Order in glassy systems *J. Phys. A: Math. Theor.* **44** 035001
[150] Franz S and Parisi G 1997 Phase diagram of coupled glassy systems: a mean-field study *Phys. Rev. Lett.* **79** 2486
[151] Franklin S V and Shattuck M D 2016 *Handbook of Granular Materials* (Boca Raton, FL: CRC Press)
[152] Jaeger H M, Nagel S R and Behringer R P 1996 Granular solids, liquids and gases *Rev. Mod. Phys.* **68** 1259–73
[153] Merrow E W 1986 *A Quantitative Assessment of the R and D Requirements for Solids Processing Technology* (Santa Monica, CA: RAND) R-3216-DOE/PSSP
[154] Goldhirsch I and Zanetti G 1993 Clustering instability in dissipative gases *Phys. Rev. Lett.* **70** 1619–22
[155] Schaeffer D G 1987 Instability in the evolution equations describing incompressible granular flow *J. Differ. Equ.* **66** 19–50
[156] Pitman E B and Schaeffer D G 1987 Stability of time dependent compressible granular flow in two dimensions *Commun. Pure Appl. Math.* **40** 421–47
[157] Barker T, Schaeffer D, Bohorquez P and Gray M T 2016 Well-posed continuum equations for granular flow with compressibility and $\mu(i)$ rheology *J. Fluid Mech.* **779** 794–818
[158] Goldenberg C and Goldhirsch I 2008 Effects of friction and disorder on the quasistatic response of granular solids to a localized force *Phys. Rev.* E **77** 041303
[159] Goldenberg C, Atman A P, Claudin P, Combe G and Goldhirsch I 2006 Scale separation in granular packings: stress plateaus and fluctuations *Phys. Rev. Lett.* **96** 168001
[160] Goldenberg C and Goldhirsch I 2005 Friction enhances elasticity in granular solids *Nature* **435** 188–91
[161] Goldenberg C and Goldhirsch I 2002 Force chains, microelasticity and macroelasticity *Phys. Rev. Lett.* **89** 084302
[162] Ramola K and Chakraborty B 2017 Stress response of granular systems *J. Stat. Phys.* **169** 1–17
[163] Anderson P W 1958 Absence of diffusion in certain random lattices *Phys. Rev.* **109** 1492
[164] Olsson P and Teitel S 2007 Critical scaling of the shear viscosity at the jamming transition *Phys. Rev. Lett.* **99** 178001
[165] Heussinger C and Barrat J-L 2009 Jamming transition as probed by quasistatic shear flow *Phys. Rev. Lett.* **102** 218303
[166] Otsuki M and Hayakawa H 2011 Critical scaling near jamming transition for frictional granular particles *Phys. Rev.* E **83** 051301
[167] Otsuki M and Hayakawa H 2017 Discontinuous change of shear modulus for frictional jammed granular materials *Phys. Rev.* E **95** 062902
[168] Pouliquen O and Forterre Y 2009 A non-local rheology of dense granular flows *Phil. Trans. R. Soc.* A **367** 5091–107
[169] Seto R, Mari R, Morris J F and Denn M M 2013 Discontinuous shear thickening of frictional hard-sphere suspensions *Phys. Rev. Lett.* **111** 218301
[170] Brown E, Forman N A, Orellana C S, Zhang H, Maynor B W, Betts D E, DeSimone J M and Jaeger H M 2010 Generality of shear thickening in dense suspensions *Nat. Mater.* **9** 220–4
[171] Brown E and Jaeger H M 2014 Shear thickening in concentrated suspensions: phenomenology, mechanisms and relations to jamming *Rep. Prog. Phys.* **77** 046602
[172] Wyart M and Cates M 2014 Discontinuous shear thickening without inertia in dense non-Brownian suspensions *Phys. Rev. Lett.* **112** 098302
[173] Cates M and Wyart M 2014 Granulation and bistability in non-Brownian suspensions *Rheol. Acta* **53** 755–64
[174] Brown E and Jaeger H M 2012 The role of dilation and confining stresses in shear thickening of dense suspensions *J. Rheol.* **56** 875–923
[175] Lootens D, van Damme H, Hémar Y and Hébraud P 2005 Dilatant flow of concentrated suspensions of rough particles *Phys. Rev. Lett.* **95** 268302
[176] Heussinger C 2013 Shear thickening in granular suspensions: inter-particle friction and dynamically correlated clusters *Phys. Rev.* E **88** 050201
[177] Fernandez N, Mani R, Rinaldi D, Kadau D, Mosquet M, Lombois-Burger H, Cayer-Barrioz J, Herrmann H J, Spencer N D and Isa L 2013 Microscopic mechanism for shear thickening of non-Brownian suspensions *Phys. Rev. Lett.* **111** 108301
[178] Mari R, Seto R, Morris J F and Denn M M 2015 Nonmonotonic flow curves of shear thickening suspensions *Phys. Rev.* E **91** 052302
[179] Han E, Peters I R and Jaeger H M 2016 High-speed ultrasound imaging in dense suspensions reveals impact-activated solidification due to dynamic shear jamming *Nat. Commun.* **7** 12243

Robert P. Behringer, James B. Duke Professor of Physics at Duke University, passed away on July 10 2018, after a short illness. This review is one of the last papers that he coauthored while in residence at the Kavli Institute for Theoretical Physics at Santa Barbara in the spring of 2018 as a participant in two programs: Memory Formation in Matter and Physics of Dense Suspensions. Bob Behringer is widely known as a pioneer in the field of granular materials. His innovative research techniques and his deep physical intuition shed light into the collective behavior of the class of fragile solids and fluids, reviewed in this article. Behringer earned his Ph.D. in 1975 from Duke University. His PhD thesis was on low temperature physics, and his postdoctoral work at Bell Laboratories focused on Rayleigh- Bénard instabilities. He joined the Department of Physics at Duke University in 1982. He was named the James B. Duke Professor of Physics in 1994. Behringer has made lasting contributions to low temperature physics, Rayleigh–Bénard convection, porous media, pattern formation, chaos, nonlinear dynamics in thin fluid films, and granular media. Behringer's use of photoelastic material to measure contact forces in granular helped launch the field of granular physics in the late 1990s. "Force chains", which have become synonymous with granular materials, were stunningly visualized using photoelastic techniques. He was passionate about unearthing the physical processes that led to this collective behavior of grains, and helped develop theories of jamming and stress propagation in granular media. Behringer was a Fellow of the American Physical Society and American Association for the Advancement of Science, and won the Jesse Beams Award from the Southeastern Section of the American Physical Society.